Angle-Constrained Formation Maneuvering of Unmanned Aerial Vehicles

Liangming Chen, Jiaping Xiao, Reuben Chua Hong Lin, and Mir Feroskhan, *Member, IEEE*

***Abstract*— In a global positioning system (GPS)-denied environment, unmanned aerial vehicles (UAVs) rely on local sensing-based formation maneuvering approaches for collective motion. To improve mission efficiency by reducing the total sensing requirements on all UAVs, this article proposes a leader–follower formation maneuvering framework with two leaders, where the followers will track the two leaders and maintain a desired angle-constrained formation with respect to the leaders using direction-only measurements, i.e., removing the need for inter-UAV distance measurements for the followers. To enable the UAV formation to maneuver in translation, rotation, and scaling simultaneously, the desired formation shape is specified by a set of interior angle constraints. By assigning each UAV's yaw angle and position as the four controllable variables, an estimation-based attitude control algorithm is designed. For the UAVs' position control, the designed formation maneuvering algorithm consists of a velocity tracking part and a formation shape control part that enables the first leader UAV to control the translational maneuvering, the second leader UAV to control the rotational and scaling maneuvering, and all the follower UAVs to maintain the formation shape. Simulations and experiments on UAVs' formation maneuvering are conducted to illustrate the effectiveness of the proposed approach.**

***Index Terms*— Angle constraints, direction measurements, formation maneuvering of unmanned aerial vehicles (UAVs), leader–follower framework.**

I. Introduction

Instead of using a single unmanned aerial vehicle (UAV), a formation of multiple UAVs is preferred in the execution of various aerial missions [1], such as search and rescue [2] and surveillance and reconnaissance [3]. In most of these missions, UAVs are required to not only form a desired geometric shape but also simultaneously maneuver collectively as a group [4]. According to the sensing information available in UAVs, the measurements used for formation maneuvering can be mainly classified into three categories, namely, absolute positions, relative positions, and directions/bearings [3], [5], [6], [7], [8].

By providing a module of global positioning system (GPS) for each UAV, the formation maneuvering approach relying on absolute position measurements can be implemented as in [9]. To enable the formation to work in a GPS-denied environment such as an indoor room, a cave, or forest, the local sensing-based formation maneuvering approaches have been extensively studied recently in [10], [11], and [12]. Among these approaches, the formation maneuvering approach using relative position measurements has been extensively studied since an inter-UAV relative position has a linear property with respect to UAVs' positions [11], [12], [13], [14]. Meanwhile, the relative position measurements can be directly acquired by installing each UAV with a bulky stereo camera or a light monocular camera with direction measurement and distance approximation [11], [12], [14]. However, such an approximation, which uses the neighboring UAVs' physical dimensions to estimate the inter-UAV distances, is less precise compared to the measured direction information [13], [15], [16], [17]. Although the relative position information can also be indirectly estimated from the measurements of inter-UAV distances and each UAV's self-displacements [18], the communication requirements will be significantly increased in such a case. To increase the system's resilience and improve mission efficiency by reducing the total sensing requirements on all UAVs, the UAV formation maneuvering approach based on pure inter-UAV direction measurements [13], [19], [20] has been proposed. When only the direction measurements are available, UAVs' formation shape can be specified by inter-UAV directions or triple-UAV angles between neighboring direction vectors. However, a direction or angle constraint is inherently nonlinear with respect to the UAV's position [8], [20], [21]. Therefore, the construction of a uniquely determined direction- or angle-constrained formation needs to be governed by the theory of bearing rigidity [19], [20], [22] or angle rigidity [8], [16], [21], which has been developed recently. Second, an inter-UAV direction will vary under the UAVs' rotational maneuvering [7], [19], due to which the rotational maneuvering of direction-constrained formations may not be straightforward. Although the angle among three UAVs is invariant under the translational, rotational, and scaling maneuvering, the angle-constrained formation maneuvering algorithms have been studied only for the 2-D case [6], [23]. As the extension to the 3-D scenario is not straightforward, the angle-constrained formation maneuvering using direction-only measurements in 3-D space is worthy of detailed investigation.

Motivated by the aforementioned challenges, this article aims to achieve 3-D angle-constrained formation maneuvering for quadrotor UAVs using direction measurements. The desired formation among the UAVs is constrained by a set of interior angles under a leader–follower framework. First, the formation maneuvering is achieved for quadrotor UAVs in 3-D whose dynamic model is more challenging than the linear integrator models in 2-D [6],

Manuscript received 29 August 2022; revised 12 December 2022; accepted 19 January 2023. Date of publication 8 February 2023; date of current version 22 June 2023. The work of Mir Feroskhan was supported by the Start-Up Grant from the School of Mechanical and Aerospace Engineering, Nanyang Technological University. Recommended by Associate Editor T. Hatanaka. *(Corresponding author: Mir Feroskhan.)*

Liangming Chen is with the Center for Control Science and Technology, Southern University of Science and Technology, Shenzhen 518055, China (e-mail: chenlm6@sustech.edu.cn).

Jiaping Xiao, Reuben Chua Hong Lin, and Mir Feroskhan are with the School of Mechanical and Aerospace Engineering, Nanyang Technological University, Singapore 639798 (e-mail: jiaping001@e.ntu.edu.sg; rchua015@e.ntu.edu.sg; mir.feroskhan@ntu.edu.sg).

This article has supplementary material provided by the authors and color versions of one or more figures available at https://doi.org/10.1109/TCST.2023.3240286.

Digital Object Identifier 10.1109/TCST.2023.3240286

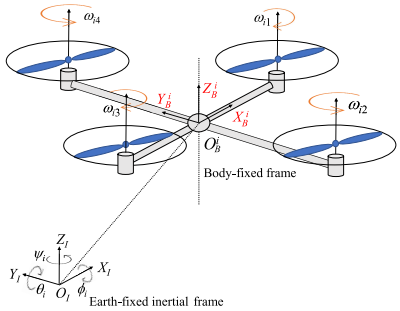

Fig. 1. Inertial frame and UAV i's body frame.

[21], [23]. Compared to the existing formation maneuvering approaches using absolute position or relative position measurements [7], [10], [13], [24], [25], our proposed approach has less requirements on sensor measurements since all follower UAVs only need direction measurements. Second, rigorous stability analysis for the angle-constrained formation maneuvering has been provided to supplement the simulation and experiment demonstration. Finally, compared to the other formation maneuvering approaches where the formation shape is specified by distances or directions [5], [7], full formation maneuvering involving translation, rotation, and scaling is achieved using our proposed angle-constrained formation maneuvering approach.

The rest of this article is organized as follows. Section II introduces the preliminaries and problem formulation. Section III discusses the partial attitude synchronization for quadrotor UAVs. The formation maneuvering algorithm and its stability analysis are given in Section IV. Some further discussions have been given in Section V. Simulation and experiment results are provided in Sections VI and VII, respectively.

II. Preliminaries and Problem Formulation

A. Attitude and Position Dynamics of Quadrotor UAVs

We consider a 3-D formation consisting of $N > 3$ quadrotor UAVs that are labeled from 1 to N. Since each UAV flies in a 3-D space and its attitude dynamics and position dynamics are coupled, we first establish the attitude and position dynamics by taking the ith quadrotor UAV as an example. As shown in Fig. 1, we define $O_I - X_I Y_I Z_I$ as the Earth-fixed inertial coordinate frame, O_B^i as the mass center of the ith quadrotor UAV, and $O_B^i - X_B^i Y_B^i Z_B^i$ as the body-fixed coordinate frame of the ith quadrotor UAV, where X_B^i and Y_B^i axes point toward two adjacent rotors of the UAV and Z_B^i follows the right-hand rule. Then, we define $p_i \in \mathbb{R}^3$ as the position of O_B^i in the inertial frame and $\Theta_i = [\phi_i, \theta_i, \psi_i]^{\mathrm{T}}$ as the ith UAV's attitude described by Euler angles with respect to $O_I - X_I Y_I Z_I$, where $\phi_i \in [0, 2\pi)$, $\theta_i \in [0, 2\pi)$, and $\psi_i \in [0, 2\pi)$ are the roll angle, pitch angle, and yaw angle, respectively. Suppose that the rotation matrix $R_i(\Theta_i)$ describes the rotation from $O_I - X_I Y_I Z_I$ to $O_B^i - X_B^i Y_B^i Z_B^i$. The position and attitude dynamics of the ith, $1 \le i \le N$, quadrotor UAV can be described as [26]

$$m_i \ddot{p}_i + m_i g z_G = u_i \tag{1}$$

$$J_i(\Theta_i)\ddot{\Theta}_i + C_i\left(\Theta_i, \dot{\Theta}_i\right)\dot{\Theta}_i = \tau_i \tag{2}$$

where $m_i \in \mathbb{R}^+$ is the UAV i's mass, $g \in \mathbb{R}$ is the gravitational acceleration constant, $z_G = [0, 0, 1]^{\mathrm{T}}$, $u_i \in \mathbb{R}^{3\times 1}$ is the applied translational control force, $\tau_i \in \mathbb{R}^{3\times 1}$ is the applied rotational control torque, and $J_i(\Theta_i) \in \mathbb{R}^{3\times 3}$ is the rotational inertia matrix of the ith UAV. The gyroscope and centrifugal terms $C_i(\Theta_i, \dot{\Theta}_i) \in \mathbb{R}^{3\times 3}$ can be described as

$$C_i\left(\Theta_i, \dot{\Theta}_i\right) = \dot{J}_i(\Theta_i) - \frac{1}{2}\frac{\partial\left(\dot{\Theta}_i^{\mathrm{T}} J_i(\Theta_i)\right)}{\partial \Theta_i} \tag{3}$$

where the detailed description of $C_i(\Theta_i, \dot{\Theta}_i)$ can be found in [27] and [26]. According to [26], the attitude dynamics (2) satisfy the following three properties.

Property 1: The inertia matrix $J_i(\Theta_i)$ is symmetric and positive definite, i.e.,

$$J_i(\Theta_i) = J_i^{\top}(\Theta_i) > 0. \tag{4}$$

Property 2: The skew-symmetric property

$$\varepsilon^T\left(\dot{J}_i(\Theta_i) - 2C_i\left(\Theta_i, \dot{\Theta}_i\right)\right)\varepsilon = 0 \ \forall \varepsilon \in \mathbb{R}^3. \tag{5}$$

Property 3: The parameter linearization property

$$J_i(\Theta_i)\,x + C_i\left(\Theta_i, \dot{\Theta}_i\right)y = Y_i\left(\Theta_i, \dot{\Theta}_i, x, y\right)\vartheta_i \ \forall x, y \in \mathbb{R}^3 \tag{6}$$

where $Y_i(\Theta_i, \dot{\Theta}_i, x, y) \in \mathbb{R}^{3\times 3}$ is a regression matrix, $\vartheta_i = [I_{11}, I_{22}, I_{33}]^{\top} \in \mathbb{R}^3$, and I_{11}, I_{22}, and I_{33} are the inertia of the ith UAV along its X_B^i-, Y_B^i-, and Z_B^i-axes, respectively.

Although the dynamics (1)–(2) have six degrees of freedom (DoFs), namely, attitude with three DoFs and position with three DoFs, a quadrotor UAV is an underactuated system since it only has four independent and controllable rotors. Therefore, only four states are fully controllable, which in this quadrotor's case are the yaw angle and the position with three DoFs. As employed in [26] and [13], an underactuated quadrotor UAV can be controlled in a cascading control architecture, in which the four rotors' speed is uniquely determined by τ_i and $\|u_i\|$. More details about the cascading control for quadrotor UAVs can be found in [26] and [13].

B. Sensor Measurements and Construction of UAVs' Desired Angle-Constrained Formation

For the attitude control, we consider that each UAV is equipped with an inertial measurement unit (IMU) to measure its own attitude angles and angular velocities with respect to the inertial coordinate frame, and wireless channels to communicate the attitude angles and angular velocities with its neighbors. For the position control, we assume that the first leader UAV is autonomous or controlled manually by an intelligent programmer such that it can navigate through the environment and guide the whole formation. As shown in Fig. 2, the second leader UAV has relative position measurement $p_2 - p_1$ with respect to the first leader UAV such that the scale of the formation can be controlled. Each follower UAV j, $j = 3, \ldots, N$, is only able to measure the direction $b_{jk} = (p_k - p_j/\|p_k - p_j\|), k \in \mathcal{N}_j$, which is a unit vector, where $\mathcal{N}_j$ represents the neighbor set of UAV j. All UAVs have velocity measurements from their onboard IMUs, which is necessary for the control of a second-order dynamical system (1) [28].

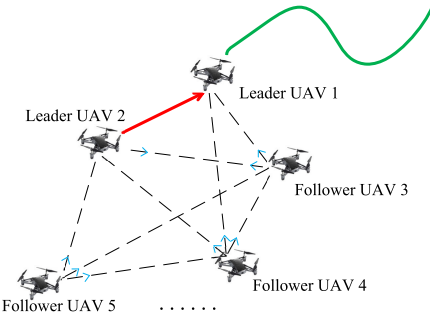

Fig. 2. Formation maneuvering structure and senor measurement topology. The red and blue arrows represent the relative position and direction measurements, respectively.

Since the UAVs' rotational maneuvering will change the inter-UAV directions, we choose interior angle constraints to describe the desired formation such that the full maneuvering of translation, rotation, and scaling can be achieved. When direction measurements b_{ij}, b_{ik} are available, the angle $\alpha_{jik} \in [0, \pi]$ that is intersected by b_{ij} and b_{ik} can be calculated by

$$\alpha_{jik} = \arccos\left(b_{ij}^{\top} b_{ik}\right) = \arccos\left(\frac{(p_j - p_i)^{\top}(p_k - p_i)}{\|p_j - p_i\|\|p_k - p_i\|}\right). \tag{7}$$

To ensure the desired angle-constrained formation shape to be uniquely determined, inspired by the construction of 2-D angle rigid formations [23], we construct the 3-D formation by a set of sequential angle constraints $\mathcal{A}^*$, which is defined as

$$\mathcal{A}^* = \Bigg\{ \underbrace{\alpha^*_{123}, \alpha^*_{231}}_{\text{first triangle}}, \quad \underbrace{\alpha^*_{423}, \alpha^*_{421}, \alpha^*_{142}}_{\text{adding UAV 4}}, \quad \ldots, \times \underbrace{\alpha^*_{ij_2j_3}, \alpha^*_{ij_2j_1}, \alpha^*_{j_1ij_2}}_{\text{adding UAV } i}, \ldots, \underbrace{\alpha^*_{Nk_2k_3}, \alpha^*_{Nk_2k_1}, \alpha^*_{k_1Nk_2}}_{\text{adding UAV } N} \Bigg\}$$

where $\alpha^*_{jik} \in (0, \pi)$ and $\{j, k\} \in \mathcal{N}_i$, $\forall \alpha^*_{jik} \in \mathcal{A}^*$. The following steps will explain how the angle constraints in $\mathcal{A}^*$ guarantee a uniquely determined formation shape [23], [29].

Step 1: Construct the first triangular shape by $\{\alpha^*_{123}, \alpha^*_{231}\}$ for the first three UAVs.

Step 2: Add the fourth UAV by $\{\alpha^*_{423}, \alpha^*_{421}, \alpha^*_{142}\}$. Since the first three UAVs' formation is uniquely determined after Step 1, we only need to check whether UAV 4's position can be fixed under the angle constrains $\{\alpha^*_{423}, \alpha^*_{421}, \alpha^*_{142}\}$. According to [23] and [29], each of the angle constraints $\{\alpha^*_{423}, \alpha^*_{421}\}$ allows UAV 4 to lie in a cone (see Fig. 3), while α^*_{142} enforces UAV 4 to lie in an arc ball, which is constructed by rotating the arc $\widehat{142}$ along the line segment $\overline{12}$ with 360 degrees (see Fig. 4). By combining Figs. 3 and Fig. 4, one has Fig. 5, which shows that UAV 4 only has two possible locations, 4 and $4'''$ (reflected with respect to plane 123) satisfying these three angle constraints $\{\alpha^*_{423}, \alpha^*_{421}, \alpha^*_{142}\}$. Since these two reflected points 4 and $4'''$ are nonadjacent, the tetrahedron formation under $\{\alpha^*_{123}, \alpha^*_{231}, \alpha^*_{423}, \alpha^*_{421}, \alpha^*_{142}\}$ is locally uniquely determined.[1]

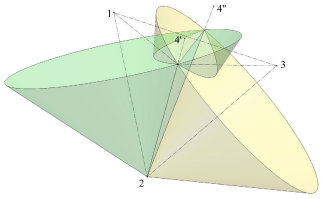

Fig. 3. Two rays intersected by two cones.

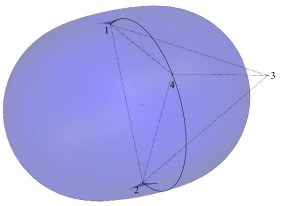

Fig. 4. Arc ball obtained by rotating the arc $\widehat{142}$ along $\overline{12}$.

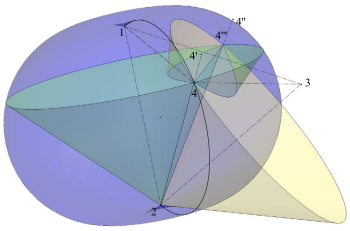

Fig. 5. Intersection of the two rays and the arc ball.

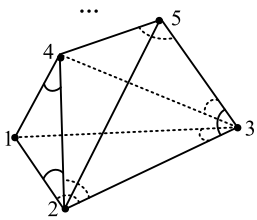

Fig. 6. Overall construction steps.

Step i − 2: Adding the ith UAV by $\{\alpha^*_{ij_2j_3}, \alpha^*_{ij_2j_1}, \alpha^*_{j_1ij_2}\}$, $j_1, j_2, j_3 \in \mathcal{N}_i$, $j_1, j_2, j_3 < i$.

Step N − 2: Adding the Nth UAV by $\{\alpha^*_{Nk_2k_3}, \alpha^*_{Nk_2k_1}, \alpha^*_{k_1Nk_2}\}$, $k_1, k_2, k_3 \in \mathcal{N}_N$, $1 \le k_1, k_2, k_3 < N$. Since the first triangular shape is unique and each of the remaining steps from 2 to $N-2$ will add one new UAV with uniquely determined position, the overall formation shape as shown in Fig. 6 is locally uniquely determined.

After the above $N-2$ steps, the desired formation is uniquely determined by the given angle constraints in $\mathcal{A}^*$. For more details about this construction, we refer the readers to [29].

C. Problem Formulation

By assuming that UAVs 1 and 2 are the two leader UAVs and the other UAVs are follower UAVs, the goal of this article is to design the control force $u_i, i = 2, \ldots, N$ for position dynamics (1) and control torque τ_i for attitude dynamics (2) such that the UAVs simultaneously achieve the two subtasks:

[1]Locally unique determination here refers to that there are two nonneighboring locations for UAV 4 under the given three angle constraints.

1) partial attitude synchronization and 2) formation maneuvering, which consists of maintaining a desired formation shape described by the interior angle constrains in $\mathcal{A}^*$, achieving a desired relative position from UAV 2 to UAV 1, and tracking the leader UAV 1's velocity. We describe these two control objectives more specifically as follows.

1) Partial Attitude Synchronization: Since each UAV is underactuated and only the yaw angle is controllable in the attitude dynamics, the aim is to design τ_i such that all the follower UAVs' yaw angles and UAV 2's yaw angle synchronize with UAV 1's yaw angle, i.e.,

$$\lim_{t\to\infty}\left(\psi_i\left(t\right)-\psi_1\left(t\right)\right)=0\ \forall i=2,\ldots,N. \tag{8}$$

2) Formation Maneuvering: The formation maneuvering task consists of two subtasks as follows.

a) Formation Shape Control: Suppose that $\delta_{12}\in\mathbb{R}^{3\times1}$ is the desired relative position of UAV 2 with respect to UAV 1, which describes the desired orientation and scale of the formation. Since the desired formation is described by δ_{12} and $\mathcal{A}^*$, the formation shape control part requires that

$$\lim_{t\to\infty}\left(p_2\left(t\right)-p_1\left(t\right)-\delta_{12}\right)=0 \tag{9}$$

$$\lim_{t\to\infty}\left(\alpha_{jik}\left(t\right)-\alpha_{jik}^*\right)=0\quad\forall\alpha_{jik}^*\in\mathcal{A}^* \tag{10}$$

where $\alpha_{jik}(t)=\arccos(b_{ij}^\top b_{ik})$ and α_{jik}^* is the desired angle formed among UAVs j,i, and k.

b) Velocity Tracking: The velocity tracking part requires the follower UAVs and UAV 2 to track the UAV 1's velocity, i.e.,

$$\lim_{t\to\infty}\left(\dot{p}_i\left(t\right)-\dot{p}_1\left(t\right)\right)=0\quad\forall i=2,\ldots,N. \tag{11}$$

Note that the formation rotational and scaling maneuvering can be achieved by adjusting the value of δ_{12} piecewise constantly [23], under which (8), (10), and (11) keep the same.

In the following, we design $\tau_i,u_i,i=2,\ldots,N$, to achieve (8)-(11) simultaneously. The following two assumptions are needed for the follow-up control design and analysis.

Assumption 1: The first leader UAV's yaw angular velocity, acceleration and jerk, and translational velocity and acceleration are bounded.

Assumption 2: The communication topology characterizing the attitude information interaction among the followers is connected and at least one follower UAV is a neighbor of the first leader. According to the neighboring rule and the defined angle set $\mathcal{A}^*$, the sensing topology describing the direction measurements is directed because if $\alpha_{jik}^*\in\mathcal{A}^*$, then we only require UAV i to be able to measure the directions b_{ij},b_{ik} such that α_{jik} can be controlled, and there is no requirement on the sensing of other inter-UAV directions.

III. Partial Attitude Synchronization

In this section, we aim at achieving (8) under the condition that UAVs can communicate with each other via a distributed network. Based on the well-known consensus algorithm, we first discuss the design of estimators for yaw angle, yaw angular velocity, and yaw angular acceleration, and subsequently use them to achieve partial attitude synchronization. Indeed, the consensus algorithms are well-known and are not the main focus of this article , but we briefly introduce them here for the completeness of the control framework of the UAVs.

A. Estimator Design for UAVs' Yaw Angles

Suppose that the first leader UAV's yaw angle $\psi_1(t)$ is time-varying and only a part of follower UAVs has the knowledge of it. Therefore, to achieve (8) for all UAVs, each UAV $i,i=2,\ldots,N$, needs to estimate $\psi_1(t)$, $\dot{\psi}_1(t)$, and $\ddot{\psi}_1(t)$, which can be realized by employing the well-known distributed estimator [30, eq. (25)]

$$\begin{aligned}\dot{\hat{\psi}}_i=&\frac{1}{\sum_{j=2}^N a_{ij}+a_{i1}}\left(\sum_{j=2}^N a_{ij}\dot{\psi}_j+a_{i1}\dot{\psi}_1\right)\\&-\frac{1}{\sum_{j=2}^N a_{ij}+a_{i1}}\times\\&\operatorname{sig}^{\gamma_1}\left(\sum_{j=2}^N a_{ij}\left(\hat{\psi}_i-\hat{\psi}_j\right)+a_{i1}\left(\hat{\psi}_i-\psi_1\right)\right)\end{aligned} \tag{12}$$

where $\hat{\psi}_i\in\mathbb{R}$ represents UAV i's estimate of ψ_1, $\operatorname{sig}(x)^{\gamma_1}=[\operatorname{sgn}(x_1)|x_1|^{\gamma_1},\ldots,\operatorname{sgn}(x_n)|x_n|^{\gamma_1}]^\top$ for any vector $x=[x_1,\ldots,x_n]^\top,0<\gamma_1<1$, sgn() represents the signum function, and $a_{ij}=1$ if j is a neighbor of i in the communication topology; otherwise, $a_{ij}=0$. Then, according to [30, Th. 14], if the UAVs' communication topology is a tree graph with UAV 1 as the root node (this assumption is used to avoid the numerical differentiation mentioned in [30, Remark 15]), then $\exists T_1>0$ such that $\forall t\geq T_1$, $\hat{\psi}_i(t)=\psi_1(t)$. Similarly, one can also design $\hat{\dot{\psi}}_{vi}(t)$ and $\hat{\ddot{\psi}}_{ai}(t)$ such that $\exists T_2>0$ and $\exists T_3>0$, $\hat{\dot{\psi}}_{vi}(t)=\dot{\psi}_1(t),\forall t>T_2$ and $\hat{\ddot{\psi}}_{ai}(t)=\ddot{\psi}_1(t),\forall t>T_3$. Therefore, $\psi_i(t)-\hat{\psi}_i(t)$, $\dot{\psi}_i(t)-\hat{\dot{\psi}}_{vi}(t)$, and $\ddot{\psi}_i(t)-\hat{\ddot{\psi}}_{ai}(t)$ converge to zero within $\max\{T_1,T_2,T_3\}$. Since $\operatorname{sig}(x)^{\gamma_1}$ is a continuous function [31], the estimation law (12) is continuous. However, according to (12), the estimators $\hat{\dot{\psi}}_{vi}$ and $\hat{\ddot{\psi}}_{ai}$ will need the information $\ddot{\psi}_1(t)$ and $\dddot{\psi}_1(t)$, respectively, which can be obtained from gyroscope embedded in IMUs with some auxiliary sensors and filtering techniques [32]. In case the measurements $\ddot{\psi}_1,\dddot{\psi}_1$ are unavailable, one alternative solution is to employ sliding-mode estimators, which may induce the chattering effect due to the usage of sgn() function. The other alternative solution is by replacing the estimators' required information $\psi_1,\dot{\psi}_1,\ddot{\psi}_1$, and $\dddot{\psi}_1$ with $\psi_1^d,\dot{\psi}_1^d,\ddot{\psi}_1^d$, and $\dddot{\psi}_1^d$, respectively, where ψ_1^d represents the desired yaw angle of the first UAV. This is because in most practical cases, the guiding UAV will be assigned to track a low-order polynomial-specified trajectory and yaw angle that are provided by a high-level motion planning algorithm, under which $\psi_1^d,\dot{\psi}_1^d,\ddot{\psi}_1^d$, and $\dddot{\psi}_1^d$ are explicitly available. Moreover, in many practical tasks, the UAVs are required to maintain a constant yaw angle, under which $\dot{\psi}_1^d,\ddot{\psi}_1^d$, and $\dddot{\psi}_1^d$ are all zero.

Remark 1: Achieving partial synchronization (8) under a distributed communication network is a typical consensus problem, in which many interesting issues can be considered. For example, to reduce the communication frequency, an event-triggered communication mechanism can be employed for the communication among the UAVs [33]. To improve the resilience of the estimators against external

wireless attacks, a resilient updating law can be employed for the estimation [34]. It is worth mentioning that due to the typical form of the estimation law (12), these interesting issues specialized to the distributed consensus can be considered for (12) by following a similar design and analysis procedure.

B. Partial Attitude Synchronization Algorithm Design

Different from $\psi_i(t)$, the desired roll angle $\phi_i^d(t)$ and the pitch angle $\theta_i^d(t)$ are determined by the control force u_i and $\psi_i^d(t)$, where u_i will be designed later and the desired yaw angle $\psi_i^d(t) = \hat{\psi}_i(t)$ in this case. According to [26] and [35], the other two attitude angles' desired values can be calculated by

$$\phi_i^d(t) = \arcsin\left(\frac{U_{ia1}(t)\sin\left(\psi_i^d(t)\right) - U_{ia2}(t)\cos\left(\psi_i^d(t)\right)}{\|U_{ia}(t)\|}\right)$$
$$\theta_i^d(t) = \arctan\left(\frac{U_{ia1}(t)\cos\left(\psi_i^d(t)\right) + U_{ia2}(t)\sin\left(\psi_i^d(t)\right)}{U_{ia3}(t)}\right) \tag{13}$$

where $U_{ia}(t) = [U_{ia1}(t), U_{ia2}(t), U_{ia3}(t)]^\top = u_i(t)/m_i$ is calculated from the control input $u_i(t)$. Then, the overall desired attitude of UAV i can be determined by $\Theta_i^d(t) = [\phi_i^d(t), \theta_i^d(t), \psi_i^d(t)]^\top$. To achieve $\Theta_i(t) \to \Theta_i^d(t)$, based on [36] and [37], we design the partial attitude synchronization algorithm as

$$\begin{aligned}&\tau_i(t)\\ &= -k_d\left(\dot{\Theta}_i(t) - \dot{q}_{ri}(t)\right) + Y_i\left(\Theta_i(t), \dot{\Theta}_i(t), \ddot{q}_{ri}(t), \dot{q}_{ri}(t)\right)\vartheta_i,\\ &\dot{q}_{ri}(t) = \dot{\Theta}_i^d(t) - \left(\Theta_i(t) - \Theta_i^d(t)\right), i = 2, \ldots, N\end{aligned} \tag{14}$$

where $\Theta_i^d(t) = [\phi_i^d(t), \theta_i^d(t), \psi_i^d(t)]^\top$ is the UAV i's desired attitude and k_d is a positive scalar. Following the stability analysis for Euler–Lagrange systems [36], [37] with the three properties introduced in (4)–(6) and the input-to-state stability (ISS) theorem [38, Lemma 4.6], the partial attitude synchronization objective (8) is achieved, i.e., $\psi_i(t) - \psi_1(t), \forall i = 2, \ldots, N$, converge to zero asymptotically under the attitude control law (14). More details about quadrotor UAVs' attitude control can be found in, e.g., [26] and [35]. According to (13) and (14), UAVs' attitude control is related to their position control, and the reverse does not hold, which is the main idea of cascading control.

IV. Formation Maneuvering

In this section, we aim to achieve formation maneuvering task (9)–(11) simultaneously. Note that in (11), the first leader UAV's translational velocity $\dot{p}_1(t)$ is time-varying and unknown for the follower UAVs. Therefore, to achieve (11), it is necessary to first design the distributed velocity and acceleration estimators for the second UAV and the follower UAVs such that they know the desired translational velocity and acceleration. Based on (12), one can use similar estimators for UAV $i, i = 2, \ldots, N$, to obtain the desired translational velocity and acceleration. The acceleration $\ddot{p}_1$ can be obtained from accelerometers combined with some auxiliary filtering. Also, by replacing $\dot{p}_1$ and $\ddot{p}_1$ with $\dot{p}_1^d$ and $\ddot{p}_1^d$, respectively, in these two estimators, the measurements of $\dot{p}_1$ and $\ddot{p}_1$ are avoided.

With the knowledge of the desired translational velocity $\dot{p}_1(t)$ and acceleration $\ddot{p}_1(t)$, we then investigate how to achieve the formation maneuvering. According to the angle set $\mathcal{A}^*$ and (9), UAVs 2 and 3 would have a different control objective than the remaining UAVs. Therefore, we investigate the formation maneuvering control design for UAVs 2 and 3 and for the remaining UAVs separately.

A. Formation Maneuvering of the First Three UAVs

Under Assumption 1, we design the formation maneuvering algorithms for UAV 2 and UAV 3 as follows:

$$\begin{aligned}u_2(t) = m_2\big[&\hat{a}_2(t) - k_v\left(\dot{p}_2(t) - \hat{v}_2(t)\right)\\ &- k_p\left(p_2(t) - p_1(t) - \delta_{12}\right) - g z_G\big]\end{aligned} \tag{15}$$

$$\begin{aligned}u_3(t) = m_3\big[&\hat{a}_3(t) - k_v\left(\dot{p}_3(t) - \hat{v}_3(t)\right) + \left(\alpha_{123}(t) - \alpha_{123}^*\right)\\ &\times b_{31}(t) - \left(\alpha_{231}(t) - \alpha_{231}^*\right)b_{32}(t) - g z_G\big]\end{aligned} \tag{16}$$

where k_v and k_p are positive scalars and $\hat{v}_i(t), \hat{a}_i(t), i = 2, 3, \ldots, N$, are the estimation of $\dot{p}_1(t)$ and $\ddot{p}_1(t)$, respectively. Then, $\exists T_4 > 0, T_5 > 0$ such that $\hat{v}_i(t) = \dot{p}_1(t), \forall t > T_4$, and $\hat{a}_i(t) = \ddot{p}_1(t), \forall t > T_5$. Note that the control law (16) requires the communication of $\alpha_{123}(t)$ from UAV 2 to UAV 3. Now, we have the results about the formation maneuvering of the first three UAVs.

Theorem 1: Under the formation maneuvering control algorithms (15) and (16) for UAVs 2 and 3, the formation maneuvering objectives (9)–(11) for the first three UAVs are locally achieved.[2]

Proof: According to Section IV-A, one has that $\hat{v}_i(t) = \dot{p}_1(t)$ and $\hat{a}_i(t) = \ddot{p}_1(t), \forall t > \max\{T_4, T_5\}$. Following [39, Th. 3.3] and [31, Th. 2], one can similarly obtain that the system states p_i and $\dot{p}_i$, $i = 1, 2, 3$, are bounded within $t \le \max\{T_4, T_5\}$. Therefore, we only need to analyze the system stability for $t > \max\{T_4, T_5\}$, under which $\hat{v}_i(t)$ and $\hat{a}_i(t)$ can be replaced by $\dot{p}_1(t)$ and $\ddot{p}_1(t)$, respectively. By defining the error variables $\tilde{v}_i(t) = \dot{p}_i(t) - \dot{p}_1(t), i = 2, 3$, $\tilde{p}_{12}(t) = p_2(t) - p_1(t) - \delta_{12}$, $e_{123}(t) = \alpha_{123}(t) - \alpha_{123}^*$, and $e_{132}(t) = \alpha_{132}(t) - \alpha_{132}^*$, the aim of (9)–(11) is to prove that these error variables converge to zero asymptotically. Toward this end, we first proceed to obtain their dynamics, which can be calculated by

$$\dot{\tilde{v}}_2 = \ddot{p}_2(t) - \ddot{p}_1(t) = -k_v\tilde{v}_2 - k_p\tilde{p}_{12} \tag{17}$$

$$\dot{\tilde{v}}_3 = \ddot{p}_3(t) - \ddot{p}_1(t) = -k_v\tilde{v}_3 - e_{231}b_{32} + e_{123}b_{31}. \tag{18}$$

$$\dot{\tilde{p}}_{12} = \dot{p}_2 - \dot{p}_1 = \tilde{v}_2. \tag{19}$$

To obtain the dynamics of angle errors, we first use the fact

$$\begin{aligned}\frac{\mathrm{d}\left(\cos\alpha_{jik}\right)}{\mathrm{d}t} &= -\left(\sin\alpha_{jik}\right)\dot{\alpha}_{jik} = \frac{\mathrm{d}\left(b_{ij}^{\mathrm{T}}b_{ik}\right)}{\mathrm{d}t} = \dot{b}_{ij}^{\mathrm{T}}b_{ik}\\ &+ b_{ij}^{\mathrm{T}}\dot{b}_{ik} = \left[\frac{P_{b_{ij}}}{l_{ij}}\left(\dot{p}_j - \dot{p}_i\right)\right]^{\mathrm{T}}b_{ik} + b_{ij}^{\mathrm{T}}\left[\frac{P_{b_{ik}}}{l_{ik}}\left(\dot{p}_k - \dot{p}_i\right)\right]\end{aligned} \tag{20}$$

[2]Corresponding to the local stability of the closed-loop dynamics, i.e., the initial formation is close to the desired formation. Note that local stability has nothing related to the local determination introduced in Section II-B.

where $l_{ij} = \|p_j - p_i\|$ and $P_{b_{ij}} = (I_3 - b_{ij}b_{ij}^{\mathrm{T}}) \in \mathbb{R}^{3\times 3}$ is the orthogonal projection matrix of direction vector b_{ij}, and we first assume $l_{ij}(t) \neq 0, l_{ik}(t) \neq 0$, which will be analyzed later. Then, it follows:

$$\begin{aligned}\dot{e}_{123} &= -\frac{\left[P_{b_{23}}(\dot{p}_3 - \dot{p}_2)\right]^{\mathrm{T}}}{l_{23}\sin\alpha_{123}}b_{21} - b_{23}^{\mathrm{T}}\frac{P_{b_{21}}}{l_{21}\sin\alpha_{123}}(\dot{p}_1 - \dot{p}_2)\\ &= N_{123}\tilde{v}_3 - (N_{123} + N_{321})\,\tilde{v}_2 \end{aligned} \tag{21}$$

where $N_{jik} = -(b_{ij}^{\mathrm{T}}P_{b_{ik}}/l_{ik}\sin\alpha_{jik}) \in \mathbb{R}^{1\times 3}$ and we have used the fact that $\dot{p}_i - \dot{p}_j = \tilde{v}_i - \tilde{v}_j$. Similarly, one also has

$$\begin{aligned}\dot{e}_{231} &= -\frac{\left[P_{b_{32}}(\dot{p}_2 - \dot{p}_3)\right]^{\mathrm{T}}}{l_{32}\sin\alpha_{231}}b_{31} - b_{32}^{\mathrm{T}}\frac{P_{b_{31}}}{l_{31}\sin\alpha_{231}}(\dot{p}_1 - \dot{p}_3)\\ &= N_{132}\tilde{v}_2 - (N_{132} + N_{231})\,\tilde{v}_3. \end{aligned} \tag{22}$$

Summarizing (17)–(22), the compact form of the closed-loop error dynamics is

$$\dot{e}_f = \begin{bmatrix} -k_v I_6 & B_1(e_f) \\ C_1(e_f) & 0 \end{bmatrix} e_f = A_1(e_f)\,e_f \tag{23}$$

where $e_f = [\tilde{v}_2^{\top}, \tilde{v}_3^{\top}, \tilde{p}_{12}^{\top}, e_{123}, e_{231}]^{\top} \in \mathbb{R}^{11}$, $B_1(e_f) = \begin{bmatrix} -k_p I_3 & 0 & 0 \\ 0 & b_{31} & -b_{32} \end{bmatrix}$, and $C_1(e_f) = \begin{bmatrix} I_3 & 0 \\ -(N_{123}+N_{321}) & N_{123} \\ N_{132} & -(N_{132}+N_{231}) \end{bmatrix}$. Since $A_1(e_f) \in \mathbb{R}^{11\times 11}$ is state-dependent and (23) is a highly nonlinear system, we use the linearization technique to analyze its local stability around the desired equilibrium $e_f = 0$. Linearizing (23) around $e_f = 0$, one has

$$\begin{aligned}\dot{e}_f &= \left(\frac{\partial\left(A_1(e_f)\,e_f\right)}{\partial e_f}|_{e_f=0}\right)e_f = \left(A_1(e_f)\,|_{e_f=0}\right)e_f\\ &= \begin{bmatrix} -k_d I_6 & B_1^* \\ C_1^* & 0 \end{bmatrix} e_f = A_1^* e_f \end{aligned} \tag{24}$$

where $B_1^* = B_1(e_f)|_{e_f=0}, C_1^* = C_1(e_f)|_{e_f=0}$, and $A_1^* = A_1(e_f)|_{e_f=0}$ are constant matrices, and we have used the fact $((\partial x/\partial e_f(i))e_f(i))|_{e_f=0} = 0$, x is an arbitrary element of $A_1(e_f)$, and $i = 1, \ldots, 11$. Therefore, the stability of (24) depends on the distribution of the eigenvalues of the matrix A_1^*. According to the Schur complement theorem, the characteristic polynomial of A_1^* can be written by

$$\begin{aligned}|\lambda I_{14} - A_1^*| &= (\lambda + k_v)^6 \det\left[\lambda I_5 - \frac{C_1^* B_1^*}{\lambda + k_v}\right]\\ &= (\lambda + k_v)\det\left[\lambda(\lambda + k_v)\,I_5 - C_1^* B_1^*\right] \end{aligned} \tag{25}$$

which implies that A_1^* always has one stable eigenvalue $-k_v$, and the remaining ten eigenvalues are the solutions of $\det[\lambda(\lambda + k_v)I_5 - C_1^*B_1^*] = 0$. Therefore, we calculate

$$C_1^* B_1^* = \begin{bmatrix} -k_p I_3 & 0 & 0 \\ k_p\left(N_{123}^* + N_{321}^*\right) & N_{123}^* b_{31}^* & 0 \\ -k_p N_{132}^* & -N_{132}^* b_{31}^* & N_{231}^* b_{32}^* \end{bmatrix} \tag{26}$$

where $b_{ij}^* = b_{ij}|_{e_f=0}$ denotes the desired direction in the desired formation and $N_{ijk}^* = N_{ijk}|_{e_f=0}$ and we have used the fact that $N_{ijk}b_{jk} = 0, \forall i \neq j \neq k$. According to the low triangular structure in (26), the five eigenvalues of $C_1^*B_1^*$ are $-k_p, -k_p, -k_p, N_{123}^*b_{31}^* = -(\cos\alpha_{213}^* + \cos\alpha_{123}^*\cos\alpha_{132}^*/l_{23}^*\sin\alpha_{123}^*) = -(\sin\alpha_{132}^*/l_{23}^*)$, and $N_{231}^*b_{32}^* = -(\sin\alpha_{132}^*/l_{31}^*)$, which are all negative Therefore, it follows that:

$$\begin{aligned}&\det\left[\lambda(\lambda + k_v)\,I_5 - C_1^*B_1^*\right]\\ &= \begin{vmatrix} (\lambda^2+k_v\lambda+k_p)I_3 & 0 & 0 \\ k_p(N_{123}^*+N_{321}^*) & \lambda^2+k_v\lambda+\frac{\sin\alpha_{132}^*}{l_{23}^*} & 0 \\ -k_pN_{132}^* & -N_{132}^*b_{31}^* & \lambda^2+k_v\lambda+\frac{\sin\alpha_{132}^*}{l_{31}^*} \end{vmatrix}\\ &= \left[\lambda^2 + k_v\lambda + k_p\right]^3\left[\lambda^2 + k_v\lambda + \frac{\sin\alpha_{132}^*}{l_{23}^*}\right]\\ &\quad\times\left[\lambda^2 + k_v\lambda + \frac{\sin\alpha_{132}^*}{l_{31}^*}\right]. \end{aligned} \tag{27}$$

Since $k_v > 0$ and $k_p > 0$, (27) implies that the ten eigenvalues lying in $\det[\lambda(\lambda + k_v)I_5 - C_1^*B_1^*] = 0$ have negative real parts. According to (25), A_1^* is Hurwitz and has 11 stable eigenvalues, which implies that (24) is exponentially stable and (23) is locally exponentially stable. Note that the analysis (21)–(27) relies on the assumption that there is no collision among neighboring UAVs. Since no collision occurs in the initial formation, there always exists a scalar $T_6 > 0$ such that no collision occurs within $[0, T_6)$, in which the analysis (21)–(27) is valid. Following [6, Proposition 1], one can extend T_6 to infinity such that the analysis (21)–(27) is valid for $t \in [0, \infty)$. Therefore, the objectives (9)–(11) are locally achieved. ■

Note that the closed-loop dynamics (23) is well-defined when no collision and collinearity occur among the first three UAVs over the whole maneuvering process. Since the UAVs initially have different locations, there always exists a time interval in which the stability analysis from (24) to (27) is valid. Now, we discuss the extension of this time interval to infinity. Since A_1^* is Hurwitz, for any positive definite $Q_1 \in \mathbb{R}^{11\times 11}$, there always exists a positive definite $P_1 \in \mathbb{R}^{11\times 11}$ such that $P_1A_1^* + A_1^{*\top}P_1 = -Q_1$. Then, we design the Lyapunov function candidate $V_1(t) = e_f^{\top}(t)P_1e_f(t)$ whose time derivative is $\dot{V}_1(t) = -e_f^{\top}(t)Q_1e_f(t) \leq -(\lambda_{\min}(Q_1)/\lambda_{\max}(P_1))V_1(t)$, which implies that $\|e_f(t)\|^2 \leq (V_1(0)/\lambda_{\min}(P_1))e^{-(\lambda_{\min}(Q_1)/\lambda_{\max}(P_1))t}$ is exponentially stable. Following the analysis in [23], if $\|p_3(0) - p_1(0)\| > 2(\lambda_{\max}(P_1)/\lambda_{\min}(Q_1))((V_1(0)/\lambda_{\min}(P_1)))^{1/2}$, then no collision will occur among UAVs 1 and 3. Also, if $(V_1(0))^{1/2} < (\lambda_{\min}(P_1))^{1/2} * \min\{\pi - \alpha_{123}^*, \alpha_{123}^*\}$, then no collinearity will occur among UAVs 1, 2, and 3. Therefore, one can choose sufficiently large initial inter-UAV distances and sufficiently small initial errors $e_f(0)$ such that no collision and collinearity will occur. Indeed, if these are not properly chosen, the inter-UAV collision is possible in angle-constrained formations due to the absence of distance measurements in UAVs. Compared with angle-constrained formation maneuvering in 2-D [23], the dimension of state variable e_f in (24) is larger than the corresponding one in 2-D, for which their eigenvalue analysis is different.

Remark 2: In (16), the two components $(\alpha_{123}(t) - \alpha_{123}^*)b_{31}(t)$ and $-(\alpha_{231}(t) - \alpha_{231}^*)b_{32}(t)$ have different signs in front of e_{123} and e_{231}. This is because the moving direction $\overrightarrow{31}$ of UAV 3 will decrease the angle α_{123}, while the moving direction $\overrightarrow{32}$ of UAV 3 will increase the angle α_{231}. Note that if b_{31} or b_{32} in (16) is replaced by $b_{31}+b_{32}$ as investigated in 2-D

[23, eq. (54)], then the closed-loop dynamics' stability in the first triangular formation will depend on additional inequalities related to the desired formation.

Remark 3: Under the control law (15), the whole formation's scale and orientation will be determined by $\|\delta_{12}\|$ and $\delta_{12}/\|\delta_{12}\|$, respectively. When the UAV formation needs to maneuver through an environment containing obstacles, it is necessary to adjust δ_{12} such that the collision between the formation and obstacles can be avoided, see, e.g., [40, Sec. V]. To achieve obstacle avoidance, the two leader UAVs need to use their environmental perception to determine δ_{12} such that the desired rotational and scaling formation maneuvering can be correspondingly conducted. Since the adjustment usually is piecewise constant and the number of adjustments is finite, the system convergence under the piecewise constant $\delta_{12}(t)$ can be guaranteed [23].

B. Formation Maneuvering of the Remaining UAVs

After the first three UAVs achieve the desired triangular formation and maneuver with the same velocity, we now design formation maneuvering algorithms for the remaining UAVs. Instead of using bisector moving rule in 2-D [23], we design the maneuvering algorithm for UAV $i, i = 4, \ldots, N$, based on a pursuing moving rule (i.e., the moving direction to reduce an angle error is along the corresponding interagent direction)

$$u_i = m_i \Big[\hat{a}_i - k_v\left(\dot{p}_i - \hat{v}_i\right) - gz_G - \left(\alpha_{j_1 i j_2} - \alpha^*_{j_1 i j_2}\right) b_{i j_2} + \left(\alpha_{i j_2 j_1} - \alpha^*_{i j_2 j_1}\right) b_{i j_1} + \left(\alpha_{i j_2 j_3} - \alpha^*_{i j_2 j_3}\right) b_{i j_3}\Big] \tag{28}$$

where $j_1 < i, j_2 < i, j_3 < i, j_i, j_2, j_3 \in \mathcal{N}_i$, $\hat{a}_i$ is the acceleration feedforward term, $-k_v(\dot{p}_i - \hat{v}_i)$ is the velocity tracking term, $-(\alpha_{j_1 i j_2} - \alpha^*_{j_1 i j_2}) b_{i j_2} + (\alpha_{i j_2 j_1} - \alpha^*_{i j_2 j_1}) b_{i j_1} + (\alpha_{i j_2 j_3} - \alpha^*_{i j_2 j_3}) b_{i j_3}$ is the formation shape control part such that UAV i keeps a desired shape (described by $\alpha^*_{j_1 i j_2}$, $\alpha^*_{i j_2 j_1}$, and $\alpha^*_{i j_2 j_3}$) with respect to UAVs j_1, j_2, and j_3. As introduced in Section II-B, the formation construction from UAV 4 to N is a sequential form. Therefore, we first illustrate how UAV 4 can be added to the existing triangular formation and then extend the case to UAVs 5 to N. The control law for UAV 4 can be written as

$$u_4 = m_4 \left[\hat{a}_4 - k_v\left(\dot{p}_4 - \hat{v}_4\right) - gz_G - \left(\alpha_{142} - \alpha^*_{142}\right) b_{42} + \left(\alpha_{421} - \alpha^*_{421}\right) b_{41} + \left(\alpha_{423} - \alpha^*_{423}\right) b_{43}\right] \tag{29}$$

where the directions b_{41}, b_{42}, and b_{43} can be measured by UAV 4's monocular camera, and the angle information α_{421} and α_{423} can be obtained by the communication with UAV 2 because the two angles $\alpha_{421} = \arccos(b_{24}^{\mathrm{T}} b_{21})$ and $\alpha_{423} = \arccos(b_{24}^{\mathrm{T}} b_{23})$ can be measured by UAV 2.

Theorem 2: For UAVs 2–4 whose position dynamics are governed by (1), under the controllers (15), (16), and (29), if the velocity feedback gain satisfies $k_v{}^2 > 2\sin\alpha^*_{142}\sin\alpha^*_{243}/(l^*_{24}(\sin\alpha^*_{142} + \sin\alpha^*_{243}))$, then the maneuvering control objectives (10) and (11) are locally achieved for UAVs 2–4.

Proof: By defining the error variables $\tilde{v}_4(t) = \dot{p}_4(t) - \dot{p}_1(t), e_{41}(t) = \alpha_{142}(t) - \alpha^*_{142}, e_{42}(t) = \alpha_{421}(t) - \alpha^*_{421}, e_{43}(t) = \alpha_{423}(t) - \alpha^*_{423}$, the aim is to prove that these error variables converge to zero. Toward this end, we first need to obtain their dynamics. Substituting (29) into (1) yields

$$\dot{\tilde{v}}_4 = \ddot{p}_4(t) - \ddot{p}_1(t) = -k_v\tilde{v}_4 - e_{41}b_{42} + e_{42}b_{41} + e_{43}b_{43}. \tag{30}$$

Using the fact (20), one also has the angle error dynamics

$$\dot{e}_{41} = \dot{\alpha}_{142} = N_{142}\tilde{v}_2 - (N_{142} + N_{241})\,\tilde{v}_4 \tag{31}$$

$$\dot{e}_{42} = \dot{\alpha}_{124} = N_{124}\tilde{v}_4 - (N_{124} + N_{421})\,\tilde{v}_2 \tag{32}$$

$$\dot{e}_{43} = \dot{\alpha}_{324} = N_{324}\tilde{v}_4 - (N_{324} + N_{423})\,\tilde{v}_2 + N_{423}\tilde{v}_3 \tag{33}$$

where $N_{jik} = -(b_{ij}^T P_{b_{ik}}/l_{ik}\sin\alpha_{jik}) \in \mathbb{R}^{1\times 3}$. Writting (30) and (31) into a compact form, one has UAV 4's closed-loop error dynamics

$$\begin{aligned}\dot{e}_4 &= \begin{bmatrix}\dot{e}_{41} & \dot{e}_{42} & \dot{e}_{43} & \dot{\tilde{v}}_4^{\top}\end{bmatrix}^{\top}\\ &= \begin{bmatrix}0 & 0 & 0 & -N_{142}-N_{241}\\ 0 & 0 & 0 & N_{124}\\ 0 & 0 & 0 & N_{324}\\ -b_{42} & b_{41} & b_{43} & -k_v I_3\end{bmatrix} e_4\\ &\quad + \begin{bmatrix}0 & N_{142}\\ -N_{124}-N_{421} & 0\\ -N_{324}-N_{423}) & N_{423}\\ 0 & 0\end{bmatrix}\begin{bmatrix}\tilde{v}_2\\ \tilde{v}_3\end{bmatrix}\\ &= \begin{bmatrix}0 & C_2\left(e_f, e_4\right)\\ D_2\left(e_f, e_4\right) & -k_v I_3\end{bmatrix} e_4 + \bar{G}_4\left(e_f, e_4\right)\begin{bmatrix}\tilde{v}_2\\ \tilde{v}_3\end{bmatrix}\\ &= B_4\left(e_f, e_4\right) e_4 + G_4\left(e_f, e_4\right) e_f\end{aligned} \tag{34}$$

where $e_4 \in \mathbb{R}^{6\times 6}$, $B_4(e_f, e_4) \in \mathbb{R}^{6\times 6}$, $\bar{G}_4(e_f, e_4) \in \mathbb{R}^{6\times 6}$, $G_4(e_f, e_4) = \left[\bar{G}_4(e_f, e_4),\ 0_{6\times 5}\right] \in \mathbb{R}^{6\times 11}$. Since $B_4(e_f, e_4)$, $G_4(e_f, e_4)$ are state-dependent matrices, (34) is a highly nonlinear system. In the following, we use the linearization technique to analyze its local stability. Linearizing (34) around the desired equilibrium $\{e_f = 0, e_4 = 0\}$ yields

$$\begin{aligned}\dot{e}_4 &= \left(\frac{\partial\left(B_4\left(e_f, e_4\right) e_4 + G_4\left(e_f, e_4\right) e_f\right)}{\partial e_4}\Big|_{e_f=0, e_4=0}\right) * e_4\\ &\quad + \left(\frac{\partial\left(B_4\left(e_f, e_4\right) e_4 + G_4\left(e_f, e_4\right) e_f\right)}{\partial e_f}\Big|_{e_f=0, e_4=0}\right) * e_f\\ &= B_4^* e_4 + G_4^* e_f\end{aligned} \tag{35}$$

where $B_4^* = B_4(e_f, e_4)|_{e_f=0,e_4=0}$, and $G_4^* = G_4(e_f, e_4)|_{e_f=0,e_4=0}$ are constant matrices. Since we already have $\lim_{t\to\infty} e_f(t) = 0$, in order to show $\lim_{t\to\infty} e_4(t) = 0$, we need to check the distribution of the 6 eigenvalues of B_4^*. Toward this end, the characteristic polynomial of B_4^* can be written as

$$\begin{aligned}&|\lambda I_6 - B_4^*|\\ &= \begin{vmatrix}\lambda I_3 & -C_2^*\\ -D_2^* & (\lambda + k_v) I_3\end{vmatrix} = \det\left[\lambda(\lambda + k_v) I_3 - C_2^* D_2^*\right]\\ &= \begin{vmatrix}\lambda(\lambda + k_v) + \frac{\sin\alpha^*_{142}}{l^*_{14}} & -\frac{\sin\alpha^*_{142}}{l^*_{42}} & d_1\\ 0 & \lambda(\lambda + k_v) + a_1 & \frac{b_{21}^{*\top} P_{b^*_{24}} b^*_{43}}{l^*_{24}\sin\alpha^*_{421}}\\ 0 & \frac{b_{23}^{*\top} P_{b^*_{24}} b^*_{41}}{l^*_{24}\sin\alpha^*_{423}} & \lambda(\lambda + k_v) + \frac{\sin\alpha^*_{243}}{l^*_{24}}\end{vmatrix}\\ &= \left[\lambda(\lambda + k_v) + \frac{\sin\alpha^*_{142}}{l^*_{14}}\right]\\ &\quad \times \left[\left(\lambda(\lambda + k_v) + a_1\right)\left(\lambda(\lambda + k_v) + b_1\right) - c_1\right]\end{aligned} \tag{36}$$

where $C_2^* = C_2(e_f, e_4)|_{e_f=0,e_4=0}$, $D_2^* = D_2(e_f, e_4)|_{e_f=0,e_4=0}$, $a_1 = (\sin\alpha_{142}^*/l_{24}^*) > 0$, $b_1 = (\sin\alpha_{243}^*/l_{24}^*) > 0$, $c_1 = (b_{21}^{*\top} P_{b_{24}^*} b_{43}^*/l_{24}^* \sin\alpha_{421}^*)(b_{23}^{*\top} P_{b_{24}^*} b_{41}^*/l_{24}^* \sin\alpha_{423}^*)$, $d_1 = -(b_{42}^{*\top} P_{b_{41}^*} b_{43}^*/l_{14}^* \sin\alpha_{142}^*) - (b_{41}^{*\top} P_{b_{42}^*} b_{43}^*/l_{42}^* \sin\alpha_{142}^*)$, and we have used the facts that $N_{jik} = -(b_{ij}^\top P_{b_{ik}}/l_{ik}\sin\alpha_{jik})$, $N_{jik} b_{ik} = 0$, $b_{ji} P_{b_{jk}} b_{ki} = \cos\alpha_{jik} + \cos\alpha_{ijk}\cos\alpha_{ikj} = \sin\alpha_{ijk}\sin\alpha_{ikj}$ because $\alpha_{ikj} + \alpha_{ijk} + \alpha_{ikj} = \pi$. Letting $|\lambda I_6 - B_4^*| = 0$, one has that $\lambda(\lambda + k_v) + (\sin\alpha_{142}^*/l_{14}^*) = 0$ will give two solutions with negative real parts, which are stable. Now, we check the remaining four eigenvalues lying in the solutions of

$$(\lambda(\lambda + k_v) + a_1)(\lambda(\lambda + k_v) + b_1) - c_1 = 0.$$

First, we prove that $a_1 b_1 > |c_1|$. Since $b_{43} = ((p_3 - p_2) + (p_2 - p_4)/l_{43})$, $P_{b_{24}}(p_2 - p_4) = 0$, and $b_{23} = ((p_3 - p_4) + (p_4 - p_2)/l_{23})$, the numerator of c_1 in (36) can be written as

$$\begin{aligned}&\left(b_{21}^{*\mathrm{T}} P_{b_{24}^*} b_{43}^*\right)\left(b_{23}^{*\mathrm{T}} P_{b_{24}^*} b_{41}^*\right)\\ &= \frac{l_{23}^*\left(b_{21}^{*\mathrm{T}} P_{b_{24}^*} b_{23}^*\right)}{l_{43}^*}\frac{l_{43}^*\left(b_{43}^{*\mathrm{T}} P_{b_{24}^*} b_{41}^*\right)}{l_{23}^*}\\ &= \left[\cos\alpha_{123}^* - \cos\alpha_{423}^*\cos\alpha_{421}^*\right]\left[\cos\alpha_{143}^* - \cos\alpha_{142}^*\cos\alpha_{243}^*\right].\end{aligned}$$

To obtain $a_1 b_1 > |c_1|$, we can prove [29]

$$\begin{aligned}&\sin\alpha_{421}^*\sin\alpha_{423}^*\sin\alpha_{142}^*\sin\alpha_{243}^* >\\ &\quad|\cos\alpha_{123}^* - \cos\alpha_{423}^*\cos\alpha_{421}^*| \times |\cos\alpha_{143}^* - \cos\alpha_{142}^*\cos\alpha_{243}^*|\end{aligned}$$

where we have used $\sin\alpha_{jik}^* > 0$. Now, we first aim to prove

$$\sin\alpha_{421}^*\sin\alpha_{423}^* > |\cos\alpha_{123}^* - \cos\alpha_{423}^*\cos\alpha_{421}^*|. \quad (37)$$

For each tetrahedron $ijkm$, one has the facts that $\alpha_{jik}^* \in (0, \pi)$, $0 < \alpha_{123}^* + \alpha_{423}^* + \alpha_{421}^* < 2\pi$, and

$$2\pi > \alpha_{ijk}^* + \alpha_{ijm}^* > \alpha_{kjm}^* > 0, i, j, k, m \in \{1, 2, 3, 4\}.$$

Then, following the discussion for the two cases of $\cos\alpha_{123}^* - \cos\alpha_{423}^*\cos\alpha_{421}^* > 0$ and $\cos\alpha_{123}^* < \cos\alpha_{423}^*\cos\alpha_{421}^*$ in [29, Ch. 6.2.2], one can similarly have that $\sin\alpha_{421}^*\sin\alpha_{423}^* > |\cos\alpha_{123}^* - \cos\alpha_{423}^*\cos\alpha_{421}^*|$ always holds for a general tetrahedron formed by UAVs 1 to 4. The same analysis can be conducted to obtain $\sin\alpha_{421}^*\sin\alpha_{423}^* > |\cos\alpha_{123}^* - \cos\alpha_{423}^*\cos\alpha_{421}^*|$, which implies that $a_1 b_1 > |c_1|$ holds.

Using Routh-Hurwitz criterion, all the four solutions of $(\lambda(\lambda + k_v) + a_1)(\lambda(\lambda + k_v) + b_1) - c_1 = 0$ have negative real parts if the following condition holds

$$\begin{aligned}&2k_v^2\left(a_1 + b_1 + k_v^2\right)(a_1 + b_1) - 4k_v^2(a_1 b_1 - c_1)\\ &\quad - (a_1 k_v + b_1 k_v)^2\\ &= k_v^2\left[(a_1 - b_1)^2 + 2k_v^2(a_1 + b_1) + 4c_1\right] > 0. \quad (38)\end{aligned}$$

Since $4|c_1| < 4a_1 b_1$, if $k_v^2 > 2a_1 b_1/(a_1 + b_1)$, then (38) holds, i.e., the remaining four eigenvalues are stable. Therefore, all the six eigenvalues of B_4^* have negative real parts if $k_v^2 > 2\sin\alpha_{142}^*\sin\alpha_{243}^*/(l_{24}^*(\sin\alpha_{142}^* + \sin\alpha_{243}^*))$. After having that B_4^* is Hurwitz and $\lim_{t\to\infty} e_4(t) = 0$, according to the ISS theorem [38, Lemma 4.7], the dynamical system (35) is locally and asymptotically stable, i.e., the control objectives (10)–(11) achieve for UAV 4. ■

Remark 4: Although work [23] also achieves angle-constrained formation maneuvering for double integrators and the position dynamics (1) are feedback linearized as double integrators in (15), (16) and (28), the main difference between [23] and this work lies in that [23] deals with formations in 2-D, while this work deals with formations in 3-D. Specifically, for each agent $i \geq 4$, (28) employs a pursuing moving rule and inter-UAV communication to achieve three desired angles, while [23, eq. (54)] employs a bisector moving rule to achieve two desired angles without using communication. Since the designed control laws in [23, eq. (54)] and (28) are different, the employed equalities/inequalities (geometric inequalities in 2-D and 3-D) for stability analysis and the obtained stability conditions (see Theorem 2 and [23, Th. 4]) are also different.

After illustrating how UAV 4 has been added to the first triangular formation, we now extend it to N-UAV formation case by following the same step as UAV 4 for UAVs 5 to N.

Proposition 1: For UAVs 2 to N whose position dynamics are governed by (1), under the controllers (15)–(16) and (28), if the velocity feedback gain $k_v^2 > 2\sin\alpha_{j_1 i j_2}^*\sin\alpha_{j_2 i j_3}^*/(l_{j_2 i}^*(\sin\alpha_{j_1 i j_2}^* + \sin\alpha_{j_2 i j_3}^*))$, $4 \leq i \leq N$ and j_1, j_2, j_3 are UAV i's three neighbors, then the maneuvering control objectives (10)–(11) are locally achieved for UAVs 2 to N.

Since the control law (28) of UAVs 5 to N has the same structure as UAV 4, one will obtain a similar error dynamics for UAV i

$$\begin{aligned}\dot{e}_i &= \left[\dot{e}_{i1}\ \dot{e}_{i2}\ \dot{e}_{i3}\ \dot{\tilde{v}}_i^\top\right]^{\mathrm{T}}\\ &= B_i\left(e_f, e_4, \ldots, e_i\right)e_i + G_i\left(e_f, e_4, \ldots, e_i\right)\\ &\quad\times\left[e_f^\top, e_4^\top, \ldots, e_{i-1}^\top\right]^{\mathrm{T}} \quad (39)\end{aligned}$$

where $N \geq i > 4$, $B_i(e_f, e_4, \ldots, e_i) \in \mathbb{R}^{6\times 6}$, and $G_i(e_f, e_4, \ldots, e_i) \in \mathbb{R}^{6\times(6i-4)}$. Using the linearization for (39) and the facts that $e_f \to 0, e_j \to 0, \forall j = 4, 5, \ldots, i-1$, one has that (39) is locally stable if $k_v^2 > 2\sin\alpha_{j_1 i j_2}^*\sin\alpha_{j_2 i j_3}^*/(l_{j_2 i}^*(\sin\alpha_{j_1 i j_2}^* + \sin\alpha_{j_2 i j_3}^*))$. This implies that the formation maneuvering is locally achieved for UAVs 2 to N.

Remark 5: By choosing sufficiently large k_v, the gain condition $k_v^2 > 2\sin\alpha_{142}^*\sin\alpha_{243}^*/(l_{24}^*(\sin\alpha_{142}^* + \sin\alpha_{243}^*))$ required in Theorem 2 can be satisfied. Note that (29) requires UAV 4 to communicate with UAV 2 to obtain the angle information α_{421} and α_{423}. In addition, for agent 4 in the 2-D case, one has $\alpha_{143} = \alpha_{142} + \alpha_{243}$ when $\overleftrightarrow{13}$ intersects with $\overleftrightarrow{24}$, which has been used many times in deriving the angle error dynamics in [23]. However, in the 3-D, $\alpha_{143} < \alpha_{142} + \alpha_{243}$, which makes the 2-D angle error dynamics and their stability analysis invalid in this 3-D case.

Remark 6: The proposed angle-constrained formation control has the advantages of simultaneous maneuvering of translation, rotation, and scaling, and requiring no distance measurements for the follower UAVs. These advantages can be utilized in several practical situations, e.g., UAV swarm in cluttered environment requiring the capability of various maneuvering forms and micro-UAV swarm for search and rescue missions where UAVs have too small volume and power capacity to equip distance sensors. In addition, since only direction measurements are required for the follower UAVs,

the presented approach can also be used to increase formation's resilience by taking the proposed method as a backup for those algorithms requiring relative position measurements.

Remark 7: For the closed-loop dynamics (23) and (34), we have obtained its local stability in Theorems 1 and 2. However, the global stability of (23) and (34) is very challenging due to two aspects. First, different from the ground robot case [21], [41], the dimension of the states in (23) is 11, due to which the analytical tool for nonlinear system's stability, such as the Poincaré–Bendixon theorem, becomes invalid. Second, the asymmetric direction measurements and information interaction topology as shown in Fig. 2 give great difficulties in constructing a candidate Lyapunov function for (23). Nevertheless, we will use numerical tools to estimate the attraction region of the local stability of (23) and (34).

V. Discussion

In this section, we further discuss three aspects regarding the proposed maneuvering algorithm's communication requirement, sensor measurements, and robustness.

A. Reduction of Neighboring UAVs' Communication

For the designed control law (16), UAV 2 needs to send the measured angle $\alpha_{123}(t)$ to UAV 3. This is necessary under the objectives (9) and (10) because α^*_{123} and α^*_{231} are chosen in $\mathcal{A}^*$, and UAV 2 must measure the interior angle $\alpha_{123}(t)$, no matter who controls it. One may suggest that to avoid the communication from UAV 2 to UAV 3, $\alpha_{123}(t)$ can be controlled by UAV 2 instead of UAV 3. However, this is impossible because UAV 1's desired position p^*_1 is determined by the translational trajectory, and then, p^*_2 is already determined by the desired relative position constraint $\delta_{12} = p^*_2 - p^*_1$; thus, one cannot further let UAV 2 to maintain α^*_{123}. An alternative solution to avoid the communication is by modifying the objective (9) into $\lim_{t\to\infty}(p_2(t)-p_3(t)-\delta_{32}) = 0$. Then, the control laws (15) and (16) can be correspondingly modified into

$$u_2 = m_2\left[\hat{a}_2 - k_v\left(\dot{p}_2 - \hat{v}_2\right) - \left(\alpha_{123} - \alpha^*_{123}\right) b_{23} - k_p\left(p_2 - p_3 - \delta_{32}\right) - g z_G\right] \tag{40}$$

$$u_3 = m_3\left[\hat{a}_3 - k_v\left(\dot{p}_3 - \hat{v}_3\right) - \left(\alpha_{231} - \alpha^*_{231}\right) b_{32} - g z_G\right]. \tag{41}$$

However, this modified control objective is less intuitive than the control objective (9) since the formation's relative orientation with respect to the first UAV becomes unclear.

For the designed control law (28) for UAVs 4 to N, it also needs the communication of the measured $\alpha_{ij_2j_1}(t)$ and $\alpha_{ij_2j_3}(t)$ from UAV j_2 to UAV i. To avoid the communication from neighboring UAVs, one can employ these three angle constraints $\alpha^*_{j_1ij_2}$, $\alpha^*_{j_2ij_3}$, and $\alpha^*_{j_3ij_1}$, $j_1 < i$, $j_2 < i$, and $j_3 < i$ to add the UAV i into the existing formation. Then, we can modify the maneuvering law (28) into

$$u_i = m_i\left[\hat{a}_i - k_v\left(\dot{p}_i - \hat{v}_i\right) - g z_G - \left(\alpha_{j_1ij_2} - \alpha^*_{j_1ij_2}\right) b_{ij_1} - \left(\alpha_{j_2ij_3} - \alpha^*_{j_2ij_3}\right) b_{ij_2} - \left(\alpha_{j_3ij_1} - \alpha^*_{j_3ij_1}\right) b_{ij_3}\right]. \tag{42}$$

However, compared with (28), the new maneuvering law (42) has two disadvantages. The first is that according to [29, Sec. 6.2.2], the desired position p^*_i is not globally uniquely determined by $\alpha^*_{j_1ij_2}$, $\alpha^*_{j_2ij_3}$, and $\alpha^*_{j_3ij_1}$, i.e., there are several other ambiguous positions $\bar{p}^*_i \neq p^*_i$ also satisfying the three angle constraints, which easily makes the UAVs converge to an undesired or ambiguous formation. Second, by employing the analysis of closed-loop dynamics (30)–(36) under (42), the formation under (28) is stable when some additional inequalities related to $\alpha^*_{j_1ij_2}$, $\alpha^*_{j_2ij_3}$, and $\alpha^*_{j_3ij_1}$ hold. Therefore, (28) can only stabilize the formations satisfying those additional inequalities, while the control law (28) can stabilize all generic formations under large k_v.

B. Comparison of Angle- and Bearing-Constrained Formations

First, we analyze the main difference between angle-constrained formations and bearing-constrained formations. Although the shape determination by a set of angle constraints is more complex than that by bearing constraints [20], angle constraints do not vary with the UAVs' coordinate frames, while bearing constraints do. More specifically, we consider $\sum_g$ as the global coordinate frame and $\sum_i$ as UAV i's sensor measurement coordinate frame. If UAV j aims to maintain the bearing constraint b^*_{ji} with respect to UAV i and $\sum_i = \sum_j = \sum_g$, then one has $b^*_{ij} = -b^*_{ji}$. However, if $\sum_i \neq \sum_g$ due to the existence of sensing noise, then $b^{i*}_{ij} \neq b^{j*}_{ji}$ and the noise-induced bias from $\sum_i$ to $\sum_g$ is unknown, which will cause the formation unstable [21, Sec. V.B]. Different from bearing vectors whose description always depends on coordinate frames, angle constraints are scalars, which are independent of UAVs' coordinate frames [42, Sec. 8.4]. Therefore, the scalar angle α^*_{jik} remains the same even when the three UAVs' coordinate frames have different orientations. Therefore, angle-constrained formations have more robustness against the misalignment of UAVs' coordinate frames.

Then, we compare the bearing-constrained formation maneuvering proposed in [7] and this angle-constrained formation maneuvering. The local convergence of this angle-constrained formation maneuvering is more restrictive than the global convergence of the bearing-constrained formation maneuvering in [7]. However, the solution proposed in this article requires less sensor measurements since our follower UAVs only need to measure directions, while the followers in [7] need relative position measurements. In addition, by assigning a 3-D rotation matrix $R(\beta_i) \in SO(3)$, $\beta_i \in \mathbb{R}^3$ in front of each bearing constraint b^*_{ij}, $j \in \mathcal{N}_i$, the rotational maneuvering can also be additionally achieved in [7] if all the agents can use a leader–follower communication network to achieve consensus $\lim_{t\to\infty}(\beta_i(t) - \beta_j(t)) = 0, \forall i, j \in \{1, \ldots, N\}$.

C. Robustness Against External Disturbances

Due to the existence of model uncertainties, wind disturbance, and structural asymmetry, there always exists an external disturbance term in the real flight dynamics of UAVs. To take this external disturbance into consideration, we modify

the model (1) and (2) into

$$m_i \ddot{p}_i + m_i g z_G = u_i + u_{di} \tag{43}$$

$$J_i(\Theta_i)\ddot{\Theta}_i + C_i\left(\Theta_i, \dot{\Theta}_i\right)\dot{\Theta}_i = \tau_i + \tau_{di} \tag{44}$$

where $u_{di} \in \mathbb{R}^3$ and $\tau_{di} \in \mathbb{R}^3$ represent the disturbances in the position dynamics and attitude dynamics, respectively. For the well-studied attitude controller (14), a variety of control techniques in [37] and [26] can be used to suppress or mitigate the external disturbance u_{di}, which, however, may not be the case for (43) since the previously proposed angle-based controllers [6], [21], [29] have not considered the existence of disturbances. Now, we take the first three UAVs' formation controllers (15) and (16) as an example, where we assume $\|u_{di}(t)\| \le d_{\max}, i = 2, 3$ and $d_{\max} \in \mathbb{R}^+$ is sufficiently small (so that the evolution of e_f will not be out of the attraction region). Under (43), the velocity error dynamics (17) and (18) need to be modified into

$$\dot{\tilde{v}}_2 = \ddot{p}_2 - \ddot{p}_1 = -k_v\tilde{v}_2 - k_p\tilde{p}_{12} + u_{d2}/m_2$$
$$\dot{\tilde{v}}_3 = \ddot{p}_3 - \ddot{p}_1 = -k_v\tilde{v}_3 - e_{231}b_{32} + e_{123}b_{31} + u_{d3}/m_3.$$

Since the dynamics of the relative position error (19) and the dynamics of the angle errors (21)–(22) keep the same, the overall closed-loop dynamics under (43) becomes

$$\dot{e}_f = A_1\left(e_f\right)e_f + d_f \tag{45}$$

where $d_f = [u_{d2}^\top/m_2, u_{d3}^\top/m_3, 0, 0, 0]^\top$. Since $d_f(t)$ is independent of the system state e_f, the linearized dynamics of (45) around the desired equilibrium $e_f = 0$ can be written by $\dot{e}_f = A_1^* e_f + d_f$. Using the Lyapunov function $V_1(t)$ for the linearized dynamics, one has

$$\begin{aligned}\dot{V}_1(t) &= -e_f^\top(t)\,Q_1 e_f(t) + e_f^\top(t)\,d_f(t)\\ &\le -e_f^\top(t)\,Q_1 e_f(t) + \|e_f\| d_{\max}\left(m_2^{-1} + m_3^{-1}\right)\\ &\le -\left(\lambda_{\min}(Q_1) - \varepsilon_1\right)\|e_f(t)\|^2\\ &\quad + 0.25 d_{\max}^2\left(m_2^{-1} + m_3^{-1}\right)^2/\varepsilon_1\end{aligned}$$

where ε_1 can be chosen as a sufficiently small positive constant. Then, by following [38, Ch. 4.8], one has $\lim_{t\to\infty}\|e_f(t)\|^2 \le 0.25 d_{\max}^2(m_2^{-1} + m_3^{-1})^2/\varepsilon_1/(\lambda_{\min}(Q_1) - \varepsilon_1)$, which indicates that the formation error is bounded when the disturbance τ_{di} exists in (43).

VI. Simulation Results

In this section, we first analyze the attraction region of the proposed formation law. Then, the simulation results under large initial formation errors and large number of UAVs will be provided. In all figures, the units used for angles are radians.

A. Numerical Analysis on Attraction Region

As mentioned in Remark 7, we can estimate the attraction region by using numerical tools. Since the nonlinear terms in the model (1) and (2) will affect the estimation, we use the single-integrator model to estimate the attraction region of angle-based formation dynamics (23) and (34). Specifically, for the first three UAVs, since the dynamics of UAVs 1 and 2 are independent of that of UAV 3, we assume that UAVs 1 and 2 achieve their control objectives and become static at p_1 and p_2, respectively. Then, UAV 3 is controlled by $\dot{p}_3 = (\alpha_{123} - \alpha_{123}^*)b_{31} - (\alpha_{231} - \alpha_{231}^*)b_{32}$, under which the whole XOY plane only has two equilibria for UAV 3 which are symmetric with respect to the Y-axis. We use the vector field $\dot{p}_3$ to show UAV 3's velocity when UAV 3 locates at $p_3 = [x; y; 0]$. According to Fig. 7(a), the whole right-half-plane only contains one stable equilibrium, which implies a large attraction region of the dynamics (23). Note that the attraction region around the other equilibrium is similar to the attraction region around p_3^*. By considering a similar case for the remaining UAVs, we assume that UAVs 1–3 are static, and UAV 4 is controlled by $\dot{p}_4 = -(\alpha_{142} - \alpha_{142}^*)b_{42} + (\alpha_{421} - \alpha_{421}^*)b_{41} + (\alpha_{423} - \alpha_{423}^*)b_{43}$, where $p_4 = [x; y; z]$. According to the vector field in Fig. 7(b), the whole up-half-plane only contains one stable equilibrium, which implies a large attraction region of the dynamics (34).

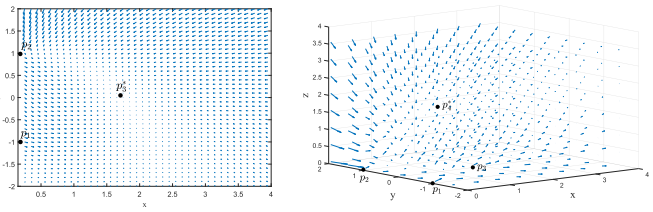

Fig. 7. Vector field of UAVs 3 and 4 under the control laws.

B. Simulation on Approximating the Formation's Stability Region Under Different Initial Errors

The stability region of the closed-loop dynamics (34) is mainly determined by the initial angle errors $\alpha_{jik}(0) - \alpha_{jik}^*, \alpha_{jik}^* \in \mathcal{A}^*$, initial relative position error $p_{12}(0) - \delta_{12}$, and initial relative velocity errors $\dot{p}_i(0) - \dot{p}_1(0), i = 2, \ldots, 5$. To approximate the stability region under different initial errors, we use five UAVs with simulation parameters $\alpha_{123}^* = \pi/4, \alpha_{231}^* = \pi/4, \alpha_{142}^* = \pi/3, \alpha_{421}^* = \pi/3, \alpha_{423}^* = \pi/3, \alpha_{253}^* = \pi/8, \alpha_{532}^* = \pi/8, \alpha_{534}^* = \pi/8$, $k_v = 5$, $\delta_{12} = [1; 2; 3]$, $\psi_1^d = 0$, and $\dot{p}_1^d = [0; 10; 0]$. We select different $p_i(0)$ and $\dot{p}_i(0), i = 1, \ldots, 5$, to produce different initial angle errors, initial relative position error, and initial relative velocity errors. The left of Fig. 8 shows the approximated stability region under different initial angle errors, which implies that the stability region is large since the range of each angle error is $(-\alpha_{jik}^*, \pi - \alpha_{jik}^*)$. The left of Fig. 8 also implies that if the first three UAVs' initial angle errors are large, then the remaining UAVs' initial angle errors should not be very close to $-\alpha_{jik}^*$, which is reasonable since the desired formation is constructed in a sequential manner. The right of Fig. 8 shows the approximated stability region under different initial angle errors and scale error, which is described by $\|p_{12}(0)\| - \|\delta_{12}\|$ (the direction of $p_{12}(0)$ is close to that of δ_{12}). The convex stability region in the right of Fig. 8 implies that the formation is unstable only when both of these two initial errors are large. We also found from simulation examples that the formation is stable when the magnitude of the UAVs' initial velocity errors varies from 0 to 100 (m/s).

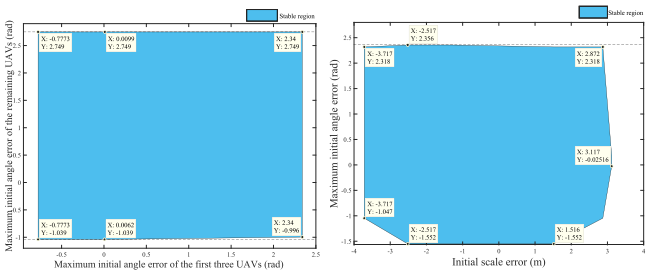

Fig. 8. Approximated stability region under different initial errors.

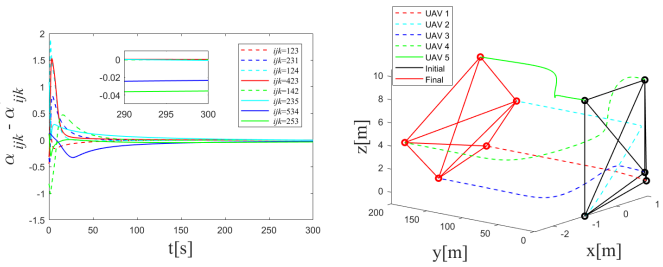

Fig. 9. Evolution of angle errors and formation trajectories.

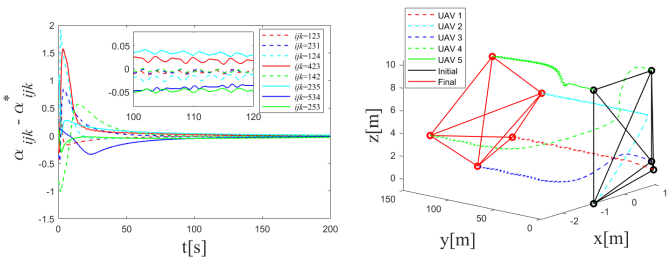

Fig. 10. Evolution of angle errors and formation trajectories.

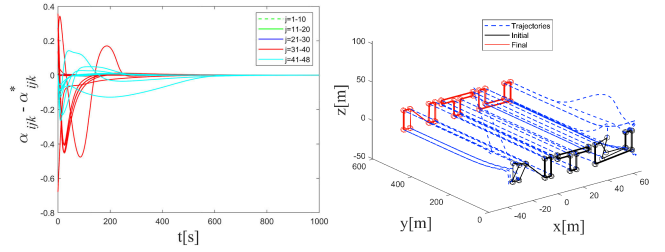

Fig. 11. Evolution of angle errors and formation trajectories.

C. Simulation Examples With Misalignment on UAVs' Coordinate Frames and Disturbances

In this section, we use the same simulation parameters as those in Section VI-B. Moreover, to validate the coordinate frame independence of angle constraints mentioned in Section V-B, we add a misalignment $\bar{R} = R_z((5\pi/180))R_y((4\pi/180))R_x((3\pi/180)) \in SO(3)$ into the follower UAV i's direction measurement coordinate frame, e.g., the term $e_{123}b_{31}$ in (16) becomes $e_{123}\bar{R}b_{31}$, where $R_x((3\pi/180))$ represents the rotation along the X-axis with $(3\pi/180)$. The simulation results are shown in Fig. 9, where the angle errors converge within 150 s. Also, to validate the robustness analyzed in Section V-C, we add each UAV i with disturbance $u_{di} = [0.2\sin(i*t), 0.2\cos(i*t), 0.1\sin(i*t)]^\top$, where $i = 1, \ldots, 5$. According to the simulation results in Fig. 10, each angle error is within 0.05 after the convergence.

D. Simulation Example With a Large Number of UAVs

To further validate that our proposed angle-constrained formation maneuvering law can work for large-scale networked UAVs, we conduct the simulation with 48 UAVs aiming to form an "NTU" shape. This desired 3-D shape is constructed by following the steps given in Section II-B, where 45 tetrahedra are used to add the UAVs 4–48 from the first triangular formation $\triangle 123$. The detailed form of these tetrahedra and the maneuvering process is given in the Supplementary Video. The convergence of some selected angle errors and formation trajectories is shown in Fig. 11. We conclude from these simulation examples in this section that the proposed angle-constrained formation maneuvering law can work well under large initial formation errors and large-scale networked UAVs.

VII. Experimental Results

In this section, we use four formation flying UAVs to validate the proposed formation maneuvering algorithms. Note that the UAVs' direction measurements are obtained from a motion capture system in our current experimental setup. The experimental videos are provided in https://www.bilibili.com/video/BV1pA411k7Xt/ and the supplementary material of this article.

A. Experimental Platform

Our experimental platform consists of four DJI Tello UAVs controlled by the received commands, a laptop computer with Wi-Fi module enabled to send commands to the UAVs using a python script, a TP-Link Router, and an OptiTrack Recording system to record the movements of the UAVs. As shown in Fig. 12, the Tello UAVs are placed in a UAV flight enclosure with 3 m height, 6 m width, and 8 m long, which lie within the sight of the OptiTrack motion capture system. As shown in Fig. 13, each UAV is attached by a holder with four markers such that it can be detected by the OptiTrack system. The OptiTrack system maps the position of each UAV into XYZ coordinates described in the system's world coordinate frame. Note that Tello SDK 2.0 [43] has provided us the movement commands (incremental form) that can be used for the translational and rotational control of the Tello UAVs. Also, the allocation and tracking of the UAVs' desired pitch and roll angles are embedded in the SDK. Therefore, in this experiment, we only need to control the position dynamics by sending the calculated formation control parts of (15), (16), and (28) to UAVs. Due to the existence of noise, a desired flying height is assigned for UAV 3, which is set as the middle of the heights of UAVs 1 and 2.

In the whole formation maneuvering process, a robot operating system (ROS) was used in the laptop computer to conduct the communication and calculation of the control commands for the UAVs. The four UAVs and the laptop computer were all connected to the TP-link router. First, the OptiTrack system acquires the positions and velocities of the four Tellos. Then, the laptop computer calculates the four Tellos' control inputs using the direction and velocity information and publishes the calculated control commands subscribed by Tello ROS nodes

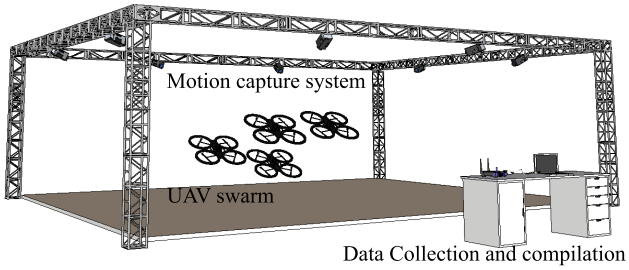

Fig. 12. Experimental platform.

Fig. 13. Tello UAVs with marker attachments.

through Wi-Fi in 500 Hz. Finally, Tello UAVs will receive the control commands, and execute them and move accordingly.

B. Experimental Parameters

In the formation experiments, the maneuvering control inputs of all four UAVs were calculated based on the information obtained from the OptiTrack system. Tello 1 is set to be the first leader UAV and its path was set to move horizontally for 3 m, under which its desired translational moving velocity is set to 0.3 m/s and desired acceleration is zero. Under this experimental setup, the communication of estimation is reduced by following the way mentioned in Section V-A, i.e., the leader UAV will send the desired moving parameters to its neighbor UAVs directly. All the other Tello UAVs are expected to follow Tello 1 while maintaining a desired formation shape. The desired position of Tello 2 with respect to Tello 1 is set to [1; 1; 0]. The desired formation angles among Tello UAVs are set as

$$\alpha^*_{123} = \frac{\pi}{4}, \quad \alpha^*_{132} = \frac{\pi}{2}, \ \alpha^*_{142} = \frac{\pi}{3}, \ \alpha^*_{421} = \frac{\pi}{3}, \ \alpha^*_{423} = \frac{\pi}{2}.$$

The control parameters are selected as $k_v = 5$ and $k_d = 8$. The updating frequency of the commands is set to be 500 Hz.

C. Experimental Results

Under the control of the designed formation maneuvering algorithms, the evolution of the angle errors and the trajectories of the four Tello UAVs in the translational maneuvering case are shown in Figs. 14–16. In addition, the scaling maneuvering and rotational maneuvering experiments are conducted to show the maneuvering capability of the proposed method, which are shown in Figs. 17 and 18, respectively.

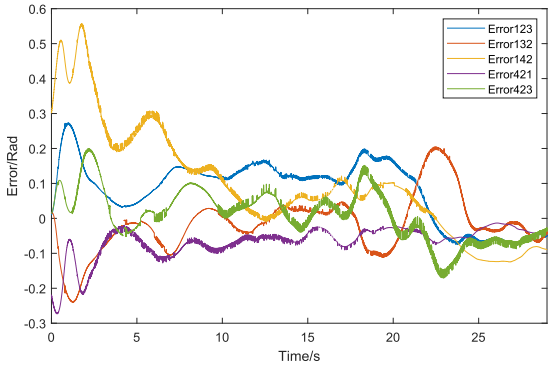

Fig. 14. Evolution of angle errors with respect to time.

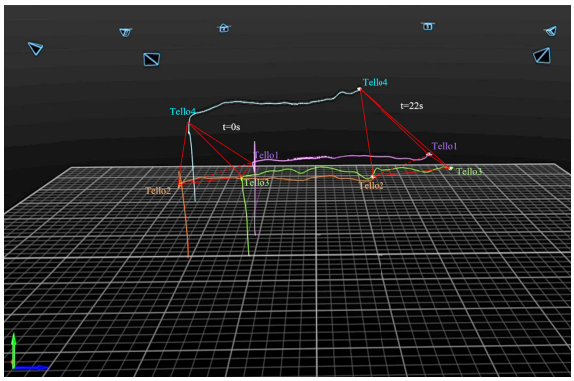

Fig. 15. 3-D view of UAV translational maneuvering trajectories recorded in OptiTrack system.

D. Analysis of Experimental Results

The experiment results in Fig. 14 show that the magnitude of the formation errors become increasingly smaller, which implies that all four UAVs converge to the desired formation. In Figs. 15 and 16, the formation shape is shown to be maintained successfully during the translational maneuvering process, which is also the case for the scaling and rotational formation maneuvering in Figs. 17 and 18.

Due to the limitation on the size of the flight enclosure, we considered that once the formation error vector is below the threshold limit of 0.1, the velocity commands of the UAVs are set to zero and the UAVs will hover on their desired spots. In order to optimize OptiTrack's localization capability of four UAVs, four different types of marker holders were designed. This ensures that OptiTrack does not mix up the UAVs during the motion capture process. The command velocities are published to the respective UAVs' ROS nodes through a while-loop block where a higher refresh rate would thus allow the UAVs to have more microcorrections per second. This allowed for better maneuvering stability during the tests of formation flight.

Finally, the control gain k_v needs to be properly selected in the experiment. According to the condition in Theorem 2, a large gain can always guarantee the maneuvering stability. However, a large gain in the experiments will give much overshoot and even make the system unstable due to the propellers' actuation saturation.

It is also interesting to apply the proposed formation strategy in the outdoor environment. We remark that one challenge of applying it in outdoor is that each UAV might not be able

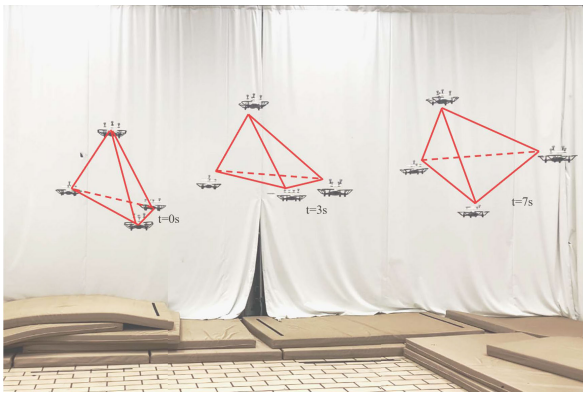

Fig. 16. Physical view of UAV translational formation maneuvering.

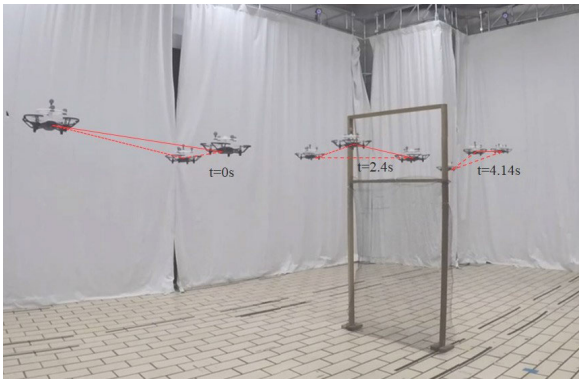

Fig. 17. Physical view of the UAV scaling formation maneuvering.

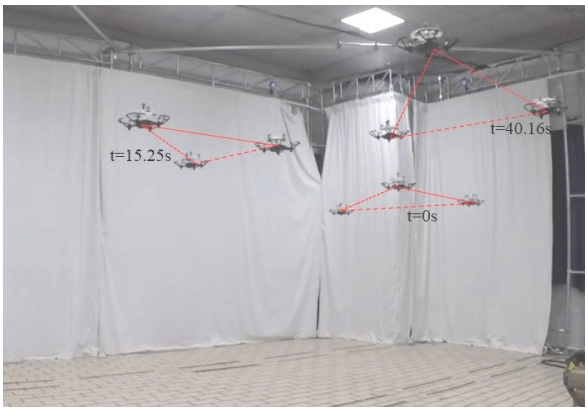

Fig. 18. Physical view of the UAV rotational formation maneuvering.

to simultaneously measure many direction measurements with respect to neighbors by using onboard sensors, e.g., cameras.

VIII. Conclusion

This article has achieved the formation maneuvering of quadrotor UAVs using direction measurements under a leader–follower framework. Each UAV's attitude and position are controlled to achieve partial attitude synchronization and desired formation maneuvering simultaneously. For the attitude part, an estimation-based attitude control algorithm has been designed to synchronize UAVs' yaw angles. For the position part, the UAVs' desired formation shape has been determined by a set of interior angle constraints. The formation maneuvering algorithm has been proposed, which consists of a velocity tracking part and a formation shape control part. Simulations and experiments have demonstrated the effectiveness of the proposed formation maneuvering control algorithms.

References

[1] Y. Zou, Z. Zhou, Z. Meng, and X. Dong, "Distributed formation control for multiple vertical takeoff and landing UAVs with switching topologies," *IEEE/ASME Trans. Mechatronics*, vol. 23, no. 4, pp. 1750–1761, Aug. 2018.

[2] E. T. Alotaibi, S. S. Alqefari, and A. Koubaa, "LSAR: Multi-UAV collaboration for search and rescue missions," *IEEE Access*, vol. 7, pp. 55817–55832, 2019.

[3] X. Dong, B. Yu, Z. Shi, and Y. Zhong, "Time-varying formation control for unmanned aerial vehicles: Theories and applications," *IEEE Trans. Control Syst. Technol.*, vol. 23, no. 1, pp. 340–348, Jan. 2015.

[4] Z. Sun, H. G. de Marina, G. S. Seyboth, B. D. O. Anderson, and C. Yu, "Circular formation control of multiple unicycle-type agents with nonidentical constant speeds," *IEEE Trans. Control Syst. Technol.*, vol. 27, no. 1, pp. 192–205, Jan. 2019.

[5] H. G. de Marina, B. Jayawardhana, and M. Cao, "Distributed rotational and translational maneuvering of rigid formations and their applications," *IEEE Trans. Robot.*, vol. 32, no. 3, pp. 684–697, Jun. 2016.

[6] L. Chen, H. G. de Marina, and M. Cao, "Maneuvering formations of mobile agents using designed mismatched angles," *IEEE Trans. Autom. Control*, vol. 67, no. 4, pp. 1655–1668, Apr. 2022.

[7] S. Zhao and D. Zelazo, "Translational and scaling formation maneuver control via a bearing-based approach," *IEEE Trans. Control Netw. Syst.*, vol. 4, no. 3, pp. 429–438, Sep. 2017.

[8] G. Jing, G. Zhang, H. W. J. Lee, and L. Wang, "Angle-based shape determination theory of planar graphs with application to formation stabilization," *Automatica*, vol. 105, pp. 117–129, Jul. 2019.

[9] G. Vásárhelyi et al., "Outdoor flocking and formation flight with autonomous aerial robots," in *Proc. IEEE/RSJ Int. Conf. Intell. Robots Syst.*, Sep. 2014, pp. 3866–3873.

[10] J. R. T. Lawton, R. W. Beard, and B. J. Young, "A decentralized approach to formation maneuvers," *IEEE Trans. Robot. Autom.*, vol. 19, no. 6, pp. 933–941, Dec. 2003.

[11] F. Lin, K. Peng, X. Dong, S. Zhao, and B. M. Chen, "Vision-based formation for UAVs," in *Proc. 11th IEEE Int. Conf. Control Autom. (ICCA)*, Jun. 2014, pp. 1375–1380.

[12] F. Schilling, F. Schiano, and D. Floreano, "Vision-based drone flocking in outdoor environments," *IEEE Robot. Autom. Lett.*, vol. 6, no. 2, pp. 2954–2961, Apr. 2021.

[13] R. Tron et al., "Vision-based formation control of aerial vehicles," in *Robotics: Science and Systems*. Philadelphia, PA, USA: Univ. of Pennsylvania Press, 2014.

[14] A. Weinstein, A. Cho, G. Loianno, and V. Kumar, "Visual inertial odometry swarm: An autonomous swarm of vision-based quadrotors," *IEEE Robot. Autom. Lett.*, vol. 3, no. 3, pp. 1801–1807, Jul. 2018.

[15] S. Zhao, Z. Li, and Z. Ding, "Bearing-only formation tracking control of multiagent systems," *IEEE Trans. Autom. Control*, vol. 64, no. 11, pp. 4541–4554, Nov. 2019.

[16] I. Buckley and M. Egerstedt, "Infinitesimal shape-similarity for characterization and control of bearing-only multirobot formations," *IEEE Trans. Robot.*, vol. 37, no. 6, pp. 1921–1935, Dec. 2021.

[17] X. Liu, S. S. Ge, and C.-H. Goh, "Vision-based leader–follower formation control of multiagents with visibility constraints," *IEEE Trans. Control Syst. Technol.*, vol. 27, no. 3, pp. 1326–1333, May 2019.

[18] T.-M. Nguyen, Z. Qiu, T. H. Nguyen, M. Cao, and L. Xie, "Persistently excited adaptive relative localization and time-varying formation of robot swarms," *IEEE Trans. Robot.*, vol. 36, no. 2, pp. 553–560, Apr. 2020.

[19] A. Franchi, C. Masone, V. Grabe, M. Ryll, H. H. Bülthoff, and P. R. Giordano, "Modeling and control of UAV bearing formations with bilateral high-level steering," *Int. J. Robot. Res.*, vol. 31, no. 12, pp. 1504–1525, Oct. 2012.

[20] S. Zhao and D. Zelazo, "Bearing rigidity and almost global bearing-only formation stabilization," *IEEE Trans. Autom. Control*, vol. 61, no. 5, pp. 1255–1268, May 2016.

[21] L. Chen, M. Cao, and C. Li, "Angle rigidity and its usage to stabilize multiagent formations in 2-D," *IEEE Trans. Autom. Control*, vol. 66, no. 8, pp. 3667–3681, Aug. 2021.

[22] T. Eren, "Formation shape control based on bearing rigidity," *Int. J. Control*, vol. 85, no. 9, pp. 1361–1379, Sep. 2012.

[23] L. Chen, M. Shi, H. G. D. Marina, and M. Cao, "Stabilizing and maneuvering angle rigid multiagent formations with double-integrator agent dynamics," *IEEE Trans. Control Netw. Syst.*, vol. 9, no. 3, pp. 1362–1374, Sep. 2022.
[24] A. Yang, W. Naeem, G. W. Irwin, and K. Li, "Stability analysis and implementation of a decentralized formation control strategy for unmanned vehicles," *IEEE Trans. Control Syst. Technol.*, vol. 22, no. 2, pp. 706–720, Mar. 2014.
[25] A. Loria, J. Dasdemir, and N. A. Jarquin, "Leader–follower formation and tracking control of mobile robots along straight paths," *IEEE Trans. Control Syst. Technol.*, vol. 24, no. 2, pp. 727–732, Mar. 2016.
[26] B. Xiao and S. Yin, "A new disturbance attenuation control scheme for quadrotor unmanned aerial vehicles," *IEEE Trans. Ind. Informat.*, vol. 13, no. 6, pp. 2922–2932, Dec. 2017.
[27] G. V. Raffo, M. G. Ortega, and F. R. Rubio, "An integral predictive/nonlinear H-infinity control structure for a quadrotor helicopter," *Automatica*, vol. 46, no. 1, pp. 29–39, 2010.
[28] J. Wang and M. Xin, "Integrated optimal formation control of multiple unmanned aerial vehicles," *IEEE Trans. Control Syst. Technol.*, vol. 21, no. 5, pp. 1731–1744, Sep. 2013.
[29] L. Chen, "Angle rigidity graph theory and multi-agent formations," Ph.D. dissertation, Dept. Sci. Eng., Univ. Groningen, Groningen, The Netherlands, 2021.
[30] S. Li, H. Du, and X. Lin, "Finite-time consensus algorithm for multi-agent systems with double-integrator dynamics," *Automatica*, vol. 47, no. 8, pp. 1706–1712, Aug. 2011.
[31] Z. Meng, W. Ren, and Z. You, "Distributed finite-time attitude containment control for multiple rigid bodies," *Automatica*, vol. 46, no. 12, pp. 2092–2099, Dec. 2010.
[32] D. Capriglione et al., "Experimental analysis of filtering algorithms for IMU-based applications under vibrations," *IEEE Trans. Instrum. Meas.*, vol. 70, pp. 1–10, 2021.
[33] D. V. Dimarogonas, E. Frazzoli, and K. H. Johansson, "Distributed event-triggered control for multi-agent systems," *IEEE Trans. Autom. Control*, vol. 57, no. 5, pp. 1291–1297, May 2012.
[34] S. Feng and H. Ishii, "Dynamic quantized consensus of general linear multi-agent systems under denial-of-service attacks," *IFAC-PapersOnLine*, vol. 53, no. 2, pp. 3533–3538, 2020.
[35] Y. Huang, W. Liu, B. Li, Y. Yang, and B. Xiao, "Finite-time formation tracking control with collision avoidance for quadrotor UAVs," *J. Franklin Inst.*, vol. 357, no. 7, pp. 4034–4058, May 2020.
[36] J. Mei, W. Ren, and G. Ma, "Distributed coordinated tracking with a dynamic leader for multiple Euler-Lagrange systems," *IEEE Trans. Autom. Control*, vol. 56, no. 6, pp. 1415–1421, Jun. 2011.
[37] R. Ortega, J. A. L. Perez, P. J. Nicklasson, and H. J. Sira-Ramirez, *Passivity-Based Control of Euler-Lagrange Systems: Mechanical, Electrical and Electromechanical Applications*. London, U.K.: Springer, 2013.
[38] H. K. Khalil, *Nonlinear Systems*, vol. 3. Upper Saddle River, NJ, USA: Prentice-Hall, 2002.
[39] J. Mei, W. Ren, and G. Ma, "Distributed containment control for Lagrangian networks with parametric uncertainties under a directed graph," *Automatica*, vol. 48, no. 4, pp. 653–659, 2012.
[40] L. Chen, J. Mei, C. Li, and G. Ma, "Distributed leader–follower affine formation maneuver control for high-order multiagent systems," *IEEE Trans. Autom. Control*, vol. 65, no. 11, pp. 4941–4948, Nov. 2020.
[41] X. Peng, Z. Sun, K. Guo, and Z. Geng, "Mobile formation coordination and tracking control for multiple nonholonomic vehicles," *IEEE/ASME Trans. Mechatronics*, vol. 25, no. 3, pp. 1231–1242, Jun. 2020.
[42] K. K. Oh, M. C. Park, and H. S. Ahn, "A survey of multi-agent formation control," *Automatica*, vol. 53, pp. 424–440, Mar. 2015.
[43] *Tello Official Website-Shenzhen Ryze Technology Co., Ltd.* Accessed: Feb. 1, 2023. [Online]. Available: https://www.ryzerobotics.com/tello-edu/downloads

Liangming Chen received the B.E. degree in automation from Southwest Jiaotong University, Chengdu, China, in 2015. He enrolled jointly in the Ph.D. program of systems and control with the Harbin Institute of Technology, Harbin, China, and the University of Groningen, Groningen, The Netherlands.

From 2021 to 2022, he was a Research Fellow with Nanyang Technological University, Singapore. He is currently an Associate Professor with the Southern University of Science and Technology, Shenzhen, China. His current research interests are in multirobot systems.

Jiaping Xiao received the B.E. degree in aircraft design and engineering and the M.S. degree in flight dynamics and control from Beihang University, Beijing, China, in 2014 and 2017, respectively. He is currently working towards the Ph.D. degree with the School of Mechanical and Aerospace Engineering, Nanyang Technological University, Singapore.

From 2017 to 2020, he was a Software Engineer with the Institute of Software, Chinese Academy of Sciences, Beijing. His research interests include machine vision and aerial robotics.

Reuben Chua Hong Lin received the B.E. degree (Hons.) in aerospace engineering from Nanyang Technological University, Singapore, in 2022.

His research interests include aerial robotics and formation control of aerial swarms.

Mir Feroskhan (Member, IEEE) received the B.E. degree (Hons.) in aerospace engineering from Nanyang Technological University (NTU), Singapore, in 2011, and the Ph.D. degree in aerospace engineering from the Florida Institute of Technology, Melbourne, FL, USA, in 2016.

He is currently an Assistant Professor with the School of Mechanical and Aerospace Engineering, NTU. His research interests include nonlinear control systems, vertical take-off and landing (VTOL) systems, unmanned aerial vehicle (UAV) design and development, flight dynamics and control, and aerial robotics.